NEUROSCIENCE

Cognitive effects of thalamostriatal degeneration are ameliorated by normalizing striatal cholinergic activity

Serena Becchi[1]*†, Billy Chieng[1]†, Laura A. Bradfield[2], Roberto Capellán[3], Beatrice K. Leung[1], Bernard W. Balleine[1]*

The loss of neurons in parafascicular thalamus (Pf) and their inputs to dorsomedial striatum (DMS) in Lewy body disease (LBD) and Parkinson's disease dementia (PDD) have been linked to the effects of neuroinflammation. We found that, in rats, these inputs were necessary for both the function of striatal cholinergic interneurons (CINs) and the flexible encoding of the action-outcome (AO) associations necessary for goal-directed action, producing a burst-pause pattern of CIN firing but only during the remapping elicited by a shift in AO contingency. Neuroinflammation in the Pf abolished these changes in CIN activity and goal-directed control after the shift in contingency. However, both effects were rescued by either the peripheral or the intra-DMS administration of selegiline, a monoamine oxidase B inhibitor that we found also enhances adenosine triphosphatase activity in CINs. These findings suggest a potential treatment for the cognitive deficits associated with neuroinflammation affecting the function of the Pf and related structures.

INTRODUCTION

The ability to encode, retrieve, and update knowledge of the consequences of our actions is necessary for goal-directed actions to remain adaptive in complex environments. Learning new strategies to achieve valued goals requires the capacity to encode specific action-outcome (AO) relationships; the accurate retrieval of which is necessary to capitalize on that information when the appropriate circumstances arise. Nevertheless, environments can change, sometimes temporarily and sometimes more permanently, and so flexibility of encoding is necessary to develop alternative strategies in these situations without necessarily erasing previously learned ones.

There is now considerable evidence that the dorsomedial striatum (DMS) serves to coordinate flexibility in the encoding and retrieval of the specific AO associations for goal-directed action in these situations (1, 2). When initially encountered, the encoding of these relations appears to depend on plasticity at direct pathway striatonigral spiny projection neurons (1), driven by activity in the corticostriatal pathway (2) and dependent on the modulatory influence of local dopamine release in this area (3). However, recent evidence suggests that remapping this learning as the environment changes depends on inputs to the DMS from the parafascicular thalamic nucleus (Pf) via the thalamostriatal pathway, which functions to control the interdigitation of newly acquired learning with previously learned strategies in a manner that reduces interference between them (4, 5).

The primary targets of the thalamostriatal pathway are the giant aspiny cholinergic interneurons (CINs) (6–8) that comprise less than 3% of striatal neurons but, through their broad arborization and mosaic distribution, generate the highest level of acetylcholine in the brain (9, 10). Pf control of the burst-pause firing pattern of CINs in the DMS (11) is vital for altering both cholinergic and dopaminergic function within targeted territories of the striatum, for encouraging or discouraging plasticity in those territories, and so for encoding newly acquired, as well as protecting preexisting, AO information when conditions in the environment change (4, 5). Thus, damage to the Pf-DMS pathway has been found to render existing and newly acquired learning subject to mutual interference, leaving animals incapable of appropriately engaging in goal-directed action control.

Given the functional importance of this pathway, its degeneration in dementia associated with Parkinson's disease (PD) and dementia with Lewy body disease (LBD), is of considerable concern (12). In PD, the progressive loss of dopaminergic neurons in the nigrostriatal pathway is accompanied by up to 30 to 40% neuronal loss in the Pf area (13–16). This latter neurodegeneration appears to be unrelated to motor deficits and contributes more to cognitive dysfunctions in LBD (17) and to the early, premotor, and advanced stages of PD when patients develop PD dementia (PDD) (18–20). Similarly, in models of PD, monkeys chronically treated with 1-methyl-4-phenyl-1,2,3,6-tetrahydropyridine (MPTP) show intralaminar thalamic degeneration and a decrease in their terminals in the striatum (17). However, preclinical studies on the neuropathological basis of PDD and LBD are rare, particularly with regard to effects on the thalamostriatal pathway, mainly because of a lack of suitable animal models for dementia-related cognitive dysfunction. Thus, the question of how to model such dysfunction in animals remains critical.

The etiology of the influence of PDD and LBD on the thalamostriatal pathway is unclear, but a role for chronic inflammation has been widely proposed as a potential mechanism (21). Neuroinflammation is increasingly considered a contributor to dementia pathogenesis (22) and is associated with the accumulation of Lewy body deposits, which are also particularly evident in the Pf area (15). Moreover, direct evidence of inflammation in LBD is growing, with elevated microglial activation identified at postmortem (23) and in vivo using positron emission tomography scan (24).

[1]School of Psychology, Faculty of Science, University of New South Wales, Sydney, Australia. [2]School of Life Sciences, Faculty of Science, University of Technology Sydney, Sydney, Australia. [3]School of Psychology, Department of Psychobiology, National University for Distance Learning, Madrid, Spain.
*Corresponding author. Email: bernard.balleine@unsw.edu.au (B.W.B.); s.becchi@unsw.edu.au (S.B.)
†These authors contributed equally to this work.

Here, we built upon this accumulating evidence to conduct a series of experiments using a disease-relevant model of cognitive dysfunction in rats, which directly relies on dysfunction of the thalamostriatal pathway, induced by targeted injections of the proinflammatory agent lipopolysaccharide (LPS) into the Pf. Given the complex dopaminergic and cholinergic profile of CIN-related modulation of striatal principal neurons, we investigated the effects of selegiline, a monoamine oxidase (MAO) inhibitor with a known cholinergic profile and originally used to palliate initial motor symptoms of early stages of PD, on the deficits in neuronal and cognitive function induced by inflammation in the Pf. We report here that the administration of selegiline during AO remapping rescues the neuronal, learning-, and memory-related deficits in goal-directed action control, normalizing CIN activity and goal-directed control after inflammation-induced damage to the Pf and Pf-DMS pathway.

RESULTS

The Pf-DMS pathway is necessary to encode changes in the AO association for goal-directed action

Considerable anatomical evidence has confirmed the existence of a direct Pf–posterior DMS (pDMS) pathway that projects unilaterally but extensively throughout all portions of the dorsal striatum (4, 25–27). Despite converging evidence that this pathway mediates the updating of AO associations (4), direct causal evidence is still lacking. In particular, it is not currently known whether this pathway mediates both the updating of learning and the retrieval of updated associations after learning. Therefore, to establish the precise role of the Pf-pDMS pathway in AO updating for our subsequent studies in this series, we first addressed this question using a chemogenetic approach. We stereotaxically injected a retro-Cre virus in the pDMS to express Cre recombinase in pDMS-projecting Pf neurons (Fig. 1A). We separated rats into four groups: In three groups, a Cre-inducible hM4 DREADD virus was stereotaxically injected into the Pf to promote the viral-mediated expression of hM4D, a Gi/o-coupled muscarinic M4 DREADD (Fig. 1, A to C). This receptor is activated by the intraperitoneal injection of an artificial ligand clozapine-N-oxide (CNO) to induce membrane hyperpolarization and neuronal silencing (28) in transfected Pf neurons projecting to pDMS, as demonstrated by ex vivo electrophysiological recording (Fig. 1, D and E, and fig. S1C for group data). A fourth group received an infusion of a null virus to serve as a CNO control.

Rats were then given behavioral training [Fig. 1F; described by Bradfield et al. (4); see Materials and Methods], with rats in groups vehicle (M4 + Vehicle), CNO control (mCherry + CNO), CNO reversal training (M4 + CNO reversal training), and CNO test (M4 + CNO test) trained to press one lever for grain pellets and a second lever for a 20% sucrose solution (counterbalanced) with reward delivered on increasing ratio schedules. All groups acquired lever pressing similarly (fig. S1A, initial identity); there was an effect of training, $F(1.629,27) = 72.06$, $P < 0.001$ (Greenhouse-Geisser corrected for violations of sphericity), which did not interact with group, $F < 1$. They were then trained on the reverse of these contingencies, i.e., if, initially, the left lever earned pellets and the right lever earned sucrose, then the left lever now earned sucrose and the right lever earned pellets. Rats in the CNO reversal training and CNO control groups received intraperitoneal injections of

CNO (7 mg/kg) 1 hour before reversal lever press sessions, whereas rats in the CNO test and vehicle groups received saline injections at the same time. Responding during the reversal stage is shown in fig. S1B (identity reversed). Again, reversal training did not differ across groups: There was an effect of training, $F(2.640,27) = 24.79$, $P < 0.001$, which did not interact with group, $F(9,81) = 1.512$, $P > 0.05$.

To evaluate what was learned after identity reversal, rats received an outcome devaluation test for which they were prefed one of the outcomes (pellets or sucrose) for 1 hour to induce sensory-specific satiety (Fig. 1F) (29). Immediately before being placed in the devaluation feeding boxes, rats in groups CNO test and CNO control received intraperitoneal injections of CNO, whereas rats in groups CNO reversal training and vehicle received intraperitoneal injections of saline. Following specific satiety induction, rats were transferred to the operant boxes for a 5-min devaluation extinction test in which both levers were extended but neither earned any outcomes. The test data are shown in Fig. 1G. From this figure, it is clear that devaluation was intact (i.e., valued > devalued) for both control groups, as well as group CNO test, but was impaired (valued = devalued) for group CNO reversal training. To analyze these data (see Materials and Methods), we first compared the control groups (vehicle and CNO control) and then the controls versus CNO test. This analysis revealed a main effect of devaluation, $F(1,27) = 12.402$, $P < 0.01$, but no interaction between either the vehicle and CNO control groups or when comparing these controls with the CNO test group ($Fs < 1$). In contrast, the comparison of these three groups with the CNO reversal training group revealed a devaluation × group interaction, $F(1,27) = 4.66$, $P = 0.040$. Follow-up simple effects analyses of this interaction confirmed that devaluation was intact (valued > devalued) for groups vehicle, $F(1,27) = 6.746$, p = 0.015; CNO control, $F(1,27) = 9.294$, $P = 0.005$; and CNO test, $F(1,27) = 4.19$ $P = 0.051$, but not for group CNO reversal training, $F < 1$. Together, these results suggest that the direct Pf → pDMS pathway is required for learning to interlace newly acquired and existing AO contingencies, but once this has been achieved, the pathway appears to be less critical for the retrieval of this information.

Effect of neuroinflammation in the Pf on cholinergic activity in the pDMS

We have explored several means of causing targeted disruption of the Pf → pDMS pathway in animal models, from excitotoxic N-methyl-D-aspartate (NMDA)–induced lesions of the Pf in the thalamus of rats (4) to chemogenetic silencing described above. In the following experiments, we assessed whether we could induce a comparable effect on this pathway using neuroinflammation. Our first model compared NMDA infusion with targeted injections of the proinflammatory agent LPS, which, when delivered in the Pf, caused a clear degeneration of the thalamostriatal pathway. This was revealed by retrograde tracing using Fluorogold (FG) (fig. S2, A to E). Immunohistological analysis revealed a decrease of FG-positive neurons in LPS- and NMDA-injected animals as compared to those receiving saline, indicating that LPS- and NMDA-induced neuronal loss included pDMS-projecting neurons in the Pf. The toxins, LPS and NMDA, and saline were injected in the Pf after FG was fully expressed (fig. S2B). Direct LPS infusion in the Pf caused microglia activation and recruitment along with neuronal loss (Fig. 2, A to D). Quantification of NeuN particles in the Pf
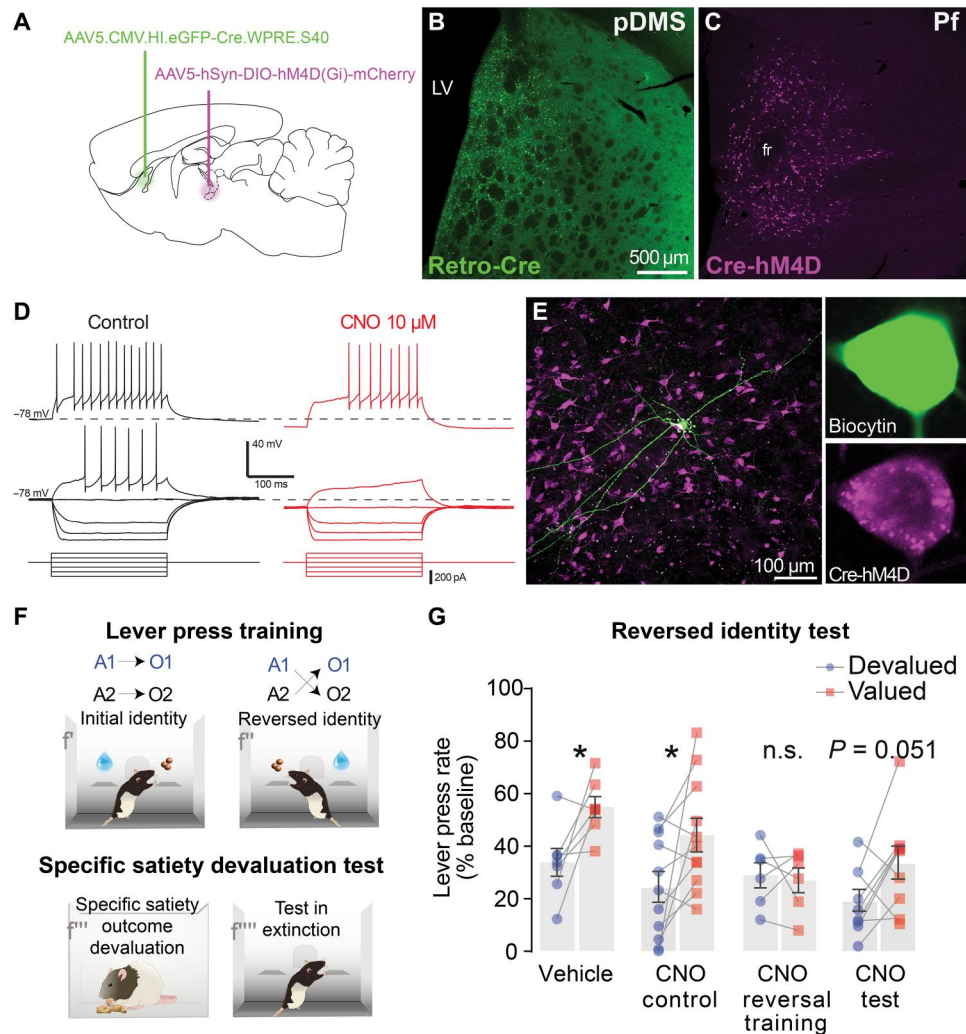
Fig. 1. The role of the Pf-DMS pathway is encoding and retrieving changes in the AO contingency. (**A**) Illustration of viral infusions given in Pf (magenta) and pDMS (green). (**B**) Representative micrographs of the injection site and the spread of retro-Cre in pDMS and (**C**) of Cre-hM4D in the Pf. (**D**) Confirmation that CNO reduced the excitability of Pf neurons expressing hM4Di ($n = 21$). Under whole-cell current clamp, the cell was resting at −78 mV before drug superfusion. A family of voltage-current relationships was then sampled by injection of incremental step current pulses. Traces were in the same cell before (left; black) and during (right; red) application of CNO (10 μM). Voltage recording from the most depolarized step is separated for clarity. (**E**) Micrograph of a biocytin-filled thalamostriatal Pf neuron from the recordings shown in (D), and in the right panels, enlargements of (E). (**F**) Design of the behavioral procedures used in this and subsequent experiments: After LPS injections in the Pf, rats were trained on two AO associations (initial identity) (f′). They were then trained on contingencies for which the outcomes associated with the two actions were reversed (reversed identity; f″). Rats were then given specific satiety-induced outcome devaluation (f‴) followed by a choice test on the two levers conducted in extinction (f‴′). (**G**) Outcome devaluation test after reversal training to assess the flexibility of goal-directed actions in rats expressing hM4D that received vehicle injections (vehicle, $n = 7$), rats with mCherry and CNO injections (CNO control, $n = 11$), rats with hM4D and CNO injections during reversal training sessions (CNO reversal training, $n = 6$), and rats with hM4D and CNO injections at test (CNO test, $n = 7$). Graphs represent means ±1 SEM; *$P < 0.05$. n.s., not significant; LV, lateral ventricle; fr, fasciculus retroflexus.

showed that LPS induced a moderate but substantial loss of NeuN-positive neurons ($P = 0.006$, unpaired t test; $t = 3.056$, df = 20; Fig. 2E). Unlike NMDA, LPS lesions in Pf were often incomplete with some small patches of viable cells (fig. S2D).

Next, we examined the effect of LPS in the Pf on the function of CINs in the pDMS. For this experiment, rats were given bilateral injections of LPS or saline. After 2 weeks, we performed patch-clamp ex vivo electrophysiology on 300-μm coronal slices centered on the pDMS. Sampling CINs in the rat pDMS based on electrophysiological characteristics, morphology, and post hoc immunohistochemistry, we found that action potential frequency was

significantly reduced in CINs recorded from the LPS-infused hemisphere compared with CINs recorded from the saline-infused hemisphere ($P = 0.038$, unpaired two-tailed t test; $t = 2.257$, df = 17; Fig. 2F). To confirm that the inflammation-induced reduction in firing rate was specific to changes in the intrinsic activity of CINs, we measured functionally relevant changes in CIN activity based on fluctuations in phosphorylation levels of the ribosomal protein S6 (p-S6rp) assessed using immunofluorescence (Fig. 2, G to I) (*30*). We quantified the state of phosphorylation of C-terminal 240 to 244 residues of ribosomal protein S6, an integrant of the ribosomal complex modulated in striatal CINs. In the hemisphere with LPS
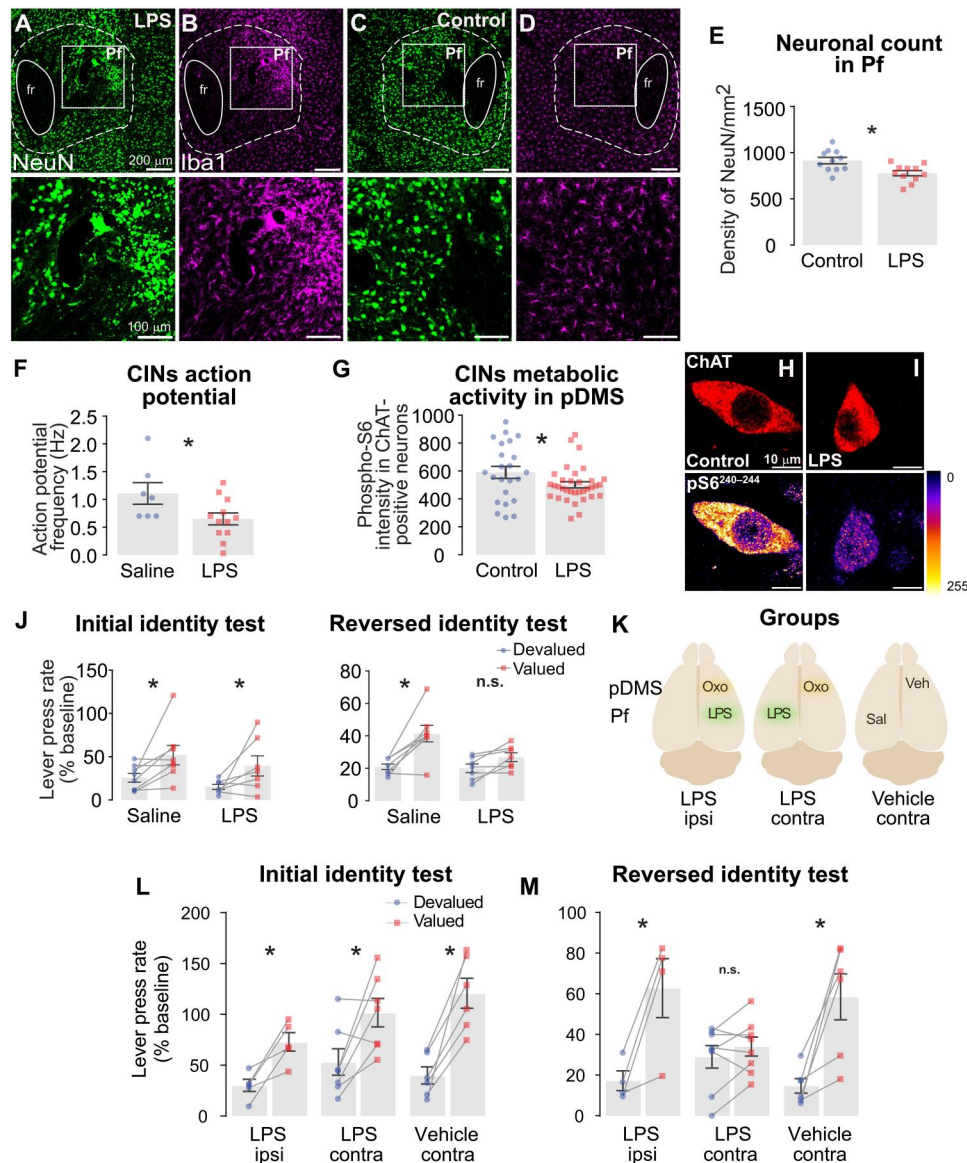
Fig. 2. Neuroinflammation in the Pf and its effect on CIN activity in the pDMS and on behavioral function. (**A** to **D**) Representative micrographs of LPS infusion (A and B) and control hemisphere (C and D) in the Pf at the top and insets shown at the bottom. Sections were labeled for microglia (Iba1; magenta) and neurons (NeuN; green). (**E**) Quantification of neuronal density in the Pf. Control, $n = 13$; LPS, $n = 13$. (**F**) Spontaneous action potential frequency in CINs sampled under cell-attached recording conditions from ex vivo brain slices taken from saline- and LPS-pretreated rats. Saline, $n = 7$; LPS, $n = 12$. (**G**) The metabolic activity of CINs calculated via quantification of p-S6rp protein activity at residues 240 to 244. Saline, $n = 23$ cells from 7 rats; LPS, $n = 34$ cells from 12 rats. (**H** and **I**) Top: Representative micrographs of CINs, identified by ChAT-positive staining (red), and p-S6rp protein expression. Bottom: A pseudo-color palette [lookup table (LUT)] highlights the intensity of p-S6rp fluorescence (display range: 0 to 255). (**J**) Outcome devaluation test after initial AO identity training (left) and after the AO identity was reversed (right) in rats that received either saline or LPS injected in the Pf. The lever press rate is expressed as a percentage of lever pressing during training (% baseline). Saline, $n = 8$; LPS, $n = 7$. (**K**) Illustration of disconnection experimental design: Rats received Oxo-S (Oxo) in the pDMS and LPS in the Pf either ipsilaterally (LPS ipsi) or contralaterally (LPS contra), the former to retain and the latter to disconnect the Pf-pDMS (CIN) pathway during reversed contingency learning. A third control group received saline (Sal) in the Pf and vehicle (Veh) in the pDMS injected contralaterally (vehicle contra). (**L**) Lever press rate, expressed as % baseline, during a choice test conducted after initial identity learning and after the outcome identities were reversed (**M**) in these same groups. Vehicle contra, $n = 6$; LPS ipsi, $n = 6$; LPS contra, $n = 9$. Error bars = ±1 SEM; *$P < 0.05$.

injection in the Pf, we detected a reduction in the p-S6rp signal in CINs in the pDMS ipsilateral to the inflammation compared to control hemispheres ($P = 0.049$, unpaired two-tailed t test; $t = 2.013$, df = 55; Fig. 2G). We then quantified the level of vGlut2 in the pDMS of animals that received LPS or saline in the Pf: No difference was found ($P > 0.05$, two-tailed unpaired t test; $t = 1.030$; df

= 20; fig. S2, F to H). In a subsequent experiment, we stereotaxically injected a retro-Cre virus in the pDMS to express Cre recombinase in pDMS-projecting Pf neurons, as well as AAV2/5-hSyn-FLEX-mGFP-2A-Synaptophysin-mRuby (Flex-mGFP-Synaptophysin-mRuby; fig. S2, I to M) in the Pf, which is able to reveal the terminal of projections from the Pf to the pDMS by showing the protein

synaptophysin in red. The mean intensity of mRuby-positive puncta was quantified, revealing a decrease in puncta in the pDMS following LPS injection in the Pf ($P = 0.039$, unpaired t test; two-tailed $t = 2.228$, df = 18; fig. S2J). Together, these results suggest that glutamatergic neurons in the Pf-pDMS pathway are sensitive to Pf inflammation, resulting in a deficit in pDMS CIN activity.

LPS-induced inflammation in the Pf impairs AO updating after a shift in contingency

We next examined the effect of bilateral infusion of LPS into the Pf on goal-directed learning after a shift in the AO contingency using outcome identity reversal. We used a similar behavioral protocol to that described above (Fig. 1F) (4). Rats given bilateral LPS or saline infusions into the Pf were food deprived and trained on a two-lever–two-outcomes procedure. Both groups learned to press the levers and increased performance with the increasing response requirement over the course of training (fig. S3A). In this study, we first assessed the encoding of the initial outcome identities using an outcome devaluation assessment before progressing to identity reversal. We found that LPS had no effect on initial AO encoding (Fig. 2J, initial identity test): Contrast analysis revealed an overall effect of devaluation $F_{(1,13)} = 9.843$, $P = 0.008$, but no main effect of group $F_{(1,13)} < 1$ and no group × devaluation interaction $F_{(1,13)} < 1$.

We then assessed the ability of the rats to update their goal-directed learning and show flexibility in AO encoding by reversing the identity of the outcomes earned by the two levers (fig. S3A, reversed). Despite the LPS group showing higher pressing rates, both groups earned an equal number of rewards during reversal training (fig. S3B). To assess what the rats learned during identity reversal, we gave them a second outcome devaluation test at the end of reversal training and found that, in marked contrast to the test after the initial learning, the LPS group failed to show an outcome devaluation effect (Fig. 2J, reversed identity test). Again, contrast analysis supported these observations, revealing a significant group × devaluation interaction, $F_{(1,13)} = 6.307$, $P = 0.026$, with simple effect analyses finding a reliable difference between devalued and valued levers in the saline group, $F_{(1,13)} = 30.808$, $P < 0.001$, but not in the LPS group, $F_{(1,13)} = 3.074$, $P > 0.05$. Thus, as found with NMDA Pf lesions (4, 31), LPS-induced neuroinflammation in the Pf impaired goal-directed action only after a change in the AO contingency.

The role of CINs in the effect of neuroinflammation in the Pf on AO remapping

To establish whether the impairment in interlacing newly acquired with existing AO associations observed in the LPS group depended on an inflammation-induced effect on cholinergic activity in the pDMS, we disconnected the Pf-pDMS pathway by infusing LPS unilaterally into the Pf before initial training and infusing oxotremorine (Oxo-S) contralaterally into the pDMS during identity reversal training. Oxo-S is a selective muscarinic agonist that binds to the muscarinic M2/M4 autoreceptors expressed on CINs (4), inhibiting the functions of these cells (4, 32–34). For this experiment, we compared a group that received LPS injected in the Pf and Oxo-S in the contralateral pDMS (LPS contra) with two control groups: one that received these infusions ipsilaterally (LPS ipsi) and a saline control (vehicle contra) that received saline infusions contralaterally (see

Fig. 2K). We conducted a direct replication of the behavioral procedures described above, and all groups responded similarly during the initial acquisition (fig. S3C) and showed evidence that they learned the initial AO associations, as revealed by an outcome devaluation test of initial identity encoding (Fig. 2L). Contrast analysis revealed a main effect of devaluation, $F_{(1,18)} = 43.386$, $P < 0.001$, but no devaluation × group interaction was found when comparing the two control groups (vehicle contra versus LPS ipsi), $F_{(1,18)} = 3.938$, $P = 0.063$, or control groups (vehicle contra + LPS ipsi) versus LPS contra, $F_{(1,18)} = 1.876$, $P = 0.188$.

Next, we trained the rats for four sessions with outcome identities reversed. Before each session of training on the newly introduced contingencies, rats were given an infusion of either Oxo-S or vehicle. As has been reported previously (4), Oxo-S produced a mild nonselective reduction in performance in both LPS ipsi and LPS contra infused groups (fig. S3C). After reversal training, rats received a drug-free outcome devaluation test. Contralateral infusions of Oxo-S during training produced a clear deficit in encoding the newly introduced AO contingency: Rats that received these infusions in pDMS contralaterally to the LPS infusion in Pf pressed both levers at a similar rate on the test, whereas rats given intra-pDMS infusions of Oxo-S ipsilaterally to Pf-LPS or vehicle rats showed a reliable outcome devaluation effect (valued > devalued; Fig. 2M, reversed identity test). Contrast analysis revealed a main effect of devaluation, $F_{(1,18)} = 47.09$, $P < 0.001$, and no interaction when comparing the two control groups (vehicle contra versus LPS ipsi) × devaluation $F < 1$. However, when the control groups combined were compared against LPS contra, this analysis revealed a significant interaction with devaluation, $F_{(1,18)} = 18.32$, $P < 0.001$. Simple effect analysis showed clear preference for the valued lever over the devalued lever in vehicle contra rats, $F_{(1,18)} = 29.049$, $P < 0.001$, and LPS ipsi rats, $F_{(1,18)} = 26.66$, $P < 0.001$, whereas performance did not differ significantly in the LPS contra rats, $F_{(1,18)} < 1$, $P > 0.05$.

Reversed contingency training increases burst-pause firing activity in CINs

Having established the importance of CINs and their function as a target of the thalamostriatal pathway, we next sought to establish how the activity of CINs is affected by activity in the Pf-pDMS pathway and, subsequently, by both initial identity training and reversed identity training. First, we infused channelrhodopsin (ChR2) into the Pf and stimulated Pf terminals in the pDMS while under whole-cell recording of a CIN. Optical illumination of the brain slice [light-emitting diode (LED) of 473 nm, 4 mW, 20 Hz, pulse duration of 5 ms] modified the regular firing of spontaneous action potentials to elicit a burst-pause firing pattern (Fig. 3, A and B); Fig. 3C shows ChR2 injection and spread.

Next, we gave two groups of rats the same amount of training except one group was maintained on the initial AO contingencies throughout, whereas the second group was given 4 days of exposure to outcome identity reversal (Fig. 3D; see fig. S3D for training data). Immediately after the final session of instrumental training, brain slices were taken for ex vivo electrophysiology. Electrophysiology was performed by an experimenter blind to the group from which the slices have been taken. Standard whole-cell patch-clamp assessment of CINs in the pDMS found a significant increase in the burst-pause pattern of action potential firing in CINs in the group given outcome identity reversal compared to rats for whom the initial
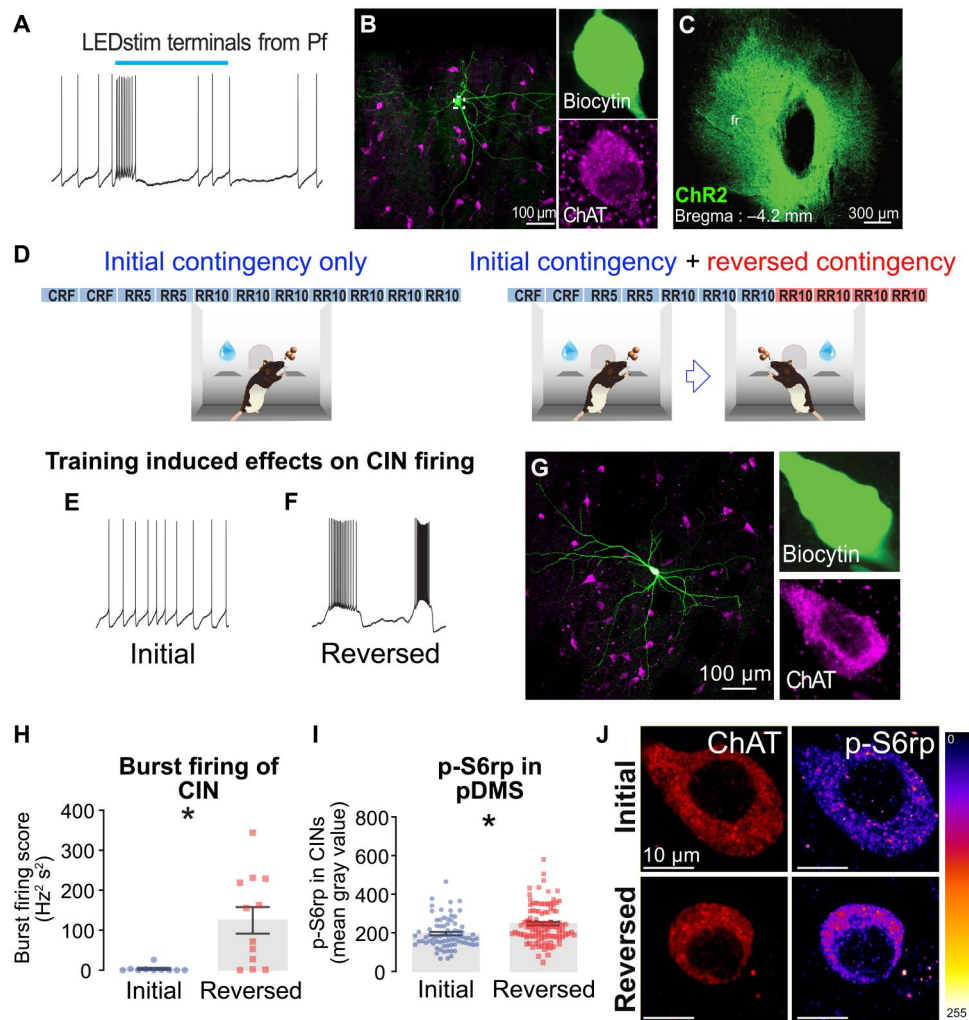
Fig. 3. Stimulation of the Pf-pDMS pathway and training on reversed AO contingencies induces burst-pause firing activity in CINs in the pDMS. (**A** and **B**) Stimulation of thalamostriatal terminals in pDMS evokes burst-pause firing in CINs. Under whole-cell recording in a CIN, optical illumination of the brain slice [light-emitting diode (LED) of 473 nm, 4 mW, 20 Hz, pulse duration of 5 ms] elicited a burst-pause firing pattern after quite regular firing of spontaneous action potentials. The blue bar on the top denotes the duration (5 s) of LED light applied (A). (B) Micrograph for the corresponding CIN recorded, typically labeled with biocytin (green) after the recording shown in (A) and post hoc histology revealing ChAT-positive immunoreactivity (magenta). On the right are enlargements of the cell body in (B). (**C**) ChR2-eYFP was injected in the Pf. (**D**) Experimental design: Half of the rats were trained on the initial AO association (left), whereas the other half were trained similarly and then given outcome identity reversal (right). (**E** and **F**) Representative voltage recording traces showing spontaneous action potential firing in CINs from rats trained under the initial (E) and reversed (F) contingencies. (**G**) A typical CIN labeled with biocytin (green) during whole-cell recording and later post hoc histology revealing ChAT-positive immunoreactivity (magenta). On the right are enlargements of the cell body. (**H**) "Burst firing score" aggregates (for analysis, see Materials and Methods) quantified from spontaneous action potential measurements under the whole-cell recording of CINs from rats trained under the initial and reversed contingencies. Initial, $n = 10$ cells from 8 rats; reversed, $n = 12$ cells from 10 rats. (**I**) CIN metabolic activity via quantification of p-S6rp. Initial, $n = 76$ cells from 10 rats; reversed, $n = 100$ cells from 10 rats. (**J**) Representative micrographs of high-magnification confocal images showing p-Ser$^{240-244}$-S6rp intensity in ChAT-immunoreactive neurons in the pDMS (red). LUT highlights the intensity of p-S6rp fluorescence (display range: 0 to 255). Error bars reflect ±1 SEM. *$P < 0.05$.

contingency was maintained (unpaired t test; $t = 3.325$, df = 20, $P = 0.003$; Fig. 3, E to H). In a separate cohort, we also found significantly higher p-S6rp immunoreactivity in CINs after reversed contingency–trained rats (unpaired t test; $t = 3.727$, df = 174, $P < 0.001$; Fig. 3, I and J). We have previously reported that p-S6rp activity at residues 240 to 244 reflects changes in CIN firing, with increased activity associated with burst firing (*30*), and although these changes in p-S6rp activity were small and their functional significance is not fully understood, they are consistent with the suggestion that the functional activity of CINs, as reflected in their burst-

pause activity, reflects the engagement of the Pf-pDMS pathway in the remapping/updating of AO encoding and the interlacing of newly acquired learning with previous learning (*35, 36*).

The MAO-B inhibitor selegiline increases burst-pause activity in CINs

We next sought to understand how changes in Pf-pDMS pathway modify the burst-pause activity of CINs. We focused on the role of dopamine, which plays a central role in most aspects of cellular activity within the striatum and particularly in striatal cholinergic

signaling and CIN excitability. Action potential firing in CINs can lead to terminal release of dopamine in the striatum via nicotinic cholinergic receptors (37). On the other hand, CINs express dopaminergic D1 and D2 receptors, as demonstrated by responses from selective receptor agonists and antagonists (4, 38–40). Elevating synaptic dopamine using cocaine has been reported to enhance the pause in CIN action potential firing, generating a more pronounced burst-pause pattern, whereas the D2 receptor antagonist sulpiride shortens the pause (36). On the basis of these findings, we first sought to explore the relationship of dopamine to burst-pause firing in CINs by comparing the effect of the MAO-B inhibitor selegiline (100 μM) with that of the MAO-A/B inhibitor pargyline (100 μM) on CIN activity in ex vivo brain slices from untrained naïve rats. Selegiline, but not pargyline, significantly increased the burst-pause firing pattern in CINs, with some neurons demonstrating a more marked effect than others (nonparametric Friedman test shows Friedman $\chi^2 = 12.67$, df = 8, $P = 0.001$; Fig. 4A). Follow-up Dunn's multiple comparison revealed a difference between baseline and selegiline ($P = 0.001$), but not between baseline and pargyline ($P > 0.05$).

To varying degrees, there is often some burst-pause and irregular firing in CINs at baseline (41, 42). However, we found that the selegiline-induced burst-pause firing pattern in CINs persisted in the presence of SCH23390 (10 μM; D1 antagonist) and raclopride (10 μM; D2 antagonist) but was blocked by the sodium-potassium adenosine triphosphatase (ATPase) blocker ouabain (100 μM; Fig. 4B), showing a reliable group effect (Friedman $\chi^2 = 8.667$, df = 8, $P = 0.010$). Dunn's multiple comparisons revealed no significant difference between the D1/D2 antagonists and selegiline ($P = 0.101$), a significant difference between ouabain and selegiline treatments ($P = 0.014$), and no difference between ouabain and D1/D2 antagonists ($P > 0.05$), suggesting that the burst-pause action potential firing evoked by selegiline was not dopamine-mediated and appeared instead to be related to a metabolic mechanism.

We have previously reported that elevated firing in CINs can increase p-S6rp immunoreactivity, a metabolic process that involves mTOR (mammalian target of rapamycin) (30). Activity in CINs is also intricately linked to the availability of adenosine triphosphate (ATP), with these neurons shutting down completely when the level of ATP is lowered by opening ATP-sensitive potassium channels (43). The routine practice of incorporating a small amount of phosphocreatine (5 to 10 mM) in the intracellular pipette solution is thought to regenerate ATP in viable brain slice experiments (44). In the present study, we found that a higher concentration of phosphocreatine (25 mM) significantly increased the burst-pause firing pattern in CINs (unpaired t test; $t = 2.685$, df = 9, $P = 0.025$; Fig. 4, C and D). In rat mesencephalic trigeminal neurons, sodium-potassium ATPase has been reported to interact with the hyperpolarization-activated cation current (I_h) (45), but we did not find any evidence that I_h in CINs was affected by selegiline application ($P > 0.05$; fig. S4). Nevertheless, selegiline's ability to increase the burst-pause firing pattern in CINs persisted in both naïve rats (Fig. 4, E, F, and I) and rats given an infusion of LPS into the Pf (Fig. 4, G, H, and J). Statistical analysis revealed that selegiline increased burst firing in both naïve rats (paired t test; $t = 2.369$, df = 10, $P = 0.0394$) and LPS-infused rats (paired t test; $t = 2.605$, df = 8, $P = 0.031$).

LPS-induced impairment in AO contingency updating is rescued by selegiline

On the basis of the finding that selegiline increases burst-pause firing in CINs, we hypothesized that its administration could rescue the behavioral impairment produced by neuroinflammation in the Pf induced by LPS infusion. To assess this hypothesis, we conducted a series of experiments in which we either injected selegiline systemically or infused it bilaterally into the pDMS during outcome identity reversal training.

In the experiment assessing peripheral selegiline, rats first received bilateral injections of LPS or saline into the Pf as described previously (Fig. 5A). After 2 weeks, rats were given instrumental training on the initial AO identities, wherein LPS rats showed similar acquisition and sensitivity to outcome devaluation to saline controls (Fig. 5B and fig. S5A): Analysis of the devaluation test showed a main effect of devaluation, $F(1,43) = 43.098$, $P < 0.001$, but no group × devaluation interaction $F < 1$. Next, rats were trained with the outcome identities reversed. Before each daily session, they received an injection of either selegiline (1 mg/kg) or saline intraperitoneally, creating four groups. Last, we assessed whether the rats were able to update the AO contingencies using a second outcome devaluation test. As is clear from Fig. 5C, whereas the devaluation effect in the saline (Sal Sal) and saline + selegiline (Sal SEL) controls did not differ, it was again abolished in the LPS Sal group. However, this debilitating effect of LPS was not observed in rats given an injection of selegiline before identity reversal training (LPS SEL), which showed a clear devaluation effect. Statistical analysis found an effect of devaluation, $F(1,42) = 27.87$, $P < 0.001$, but no interaction between the controls (Sal Sal versus Sal SEL) or between the controls combined and the LPS SEL group, ($Fs < 1$). In contrast, comparison of these three groups (Sal Sal + Sal SEL + LPS SEL) against LPS Sal found a group × devaluation interaction, $F(1,42) = 4.803$, $P = 0.034$. Follow-up simple effect analysis between devalued and valued levers revealed a significant difference in the Sal Sal group, $F(1,42) = 13.218$, $P = 0.001$; the Sal SEL group, $F(1,42) = 9.562$, $P = 0.004$; and the LPS SEL group, $F(1,42) = 9.185$, $P = 0.004$, but not the LPS Sal group, $F < 1$. To confirm the effect of intraperitoneal selegiline on CIN function in the pDMS, we examined p-S6rp intensity in choline acetyltransferase–positive (ChAT$^+$) neurons in the pDMS of rats from the four groups immediately before a fifth training session and found an increase of p-S6rp signaling after selegiline treatment (fig. S5B).

We next sought to establish whether the effect of peripherally administered selegiline could be replicated using microinfusions directly into the pDMS (see Materials and Methods). Accordingly, all groups and methods were the same as the previous experiment except selegiline or saline was locally infused into the pDMS 20 min before each outcome identity reversal training session. LPS-affected areas and cannula placements in the pDMS are shown in Fig. 5D. There were no differences in training on the initial and reversed contingencies between groups that received LPS or saline in the Pf (fig. S5B). In the first devaluation test, LPS again had no effect on goal-directed behavior: Contrast analysis revealed an overall devaluation effect, $F(1,30) = 51.30$, $P < 0.001$, but neither an effect of group or an group × devaluation interaction, $F(1,30) = 1.65$, $P > 0.05$ (Fig. 5E).

As observed using peripheral selegiline injection, we again found that selegiline was able to rescue the LPS-induced deficit in AO encoding during identity reversal. Rats given microinfusions of
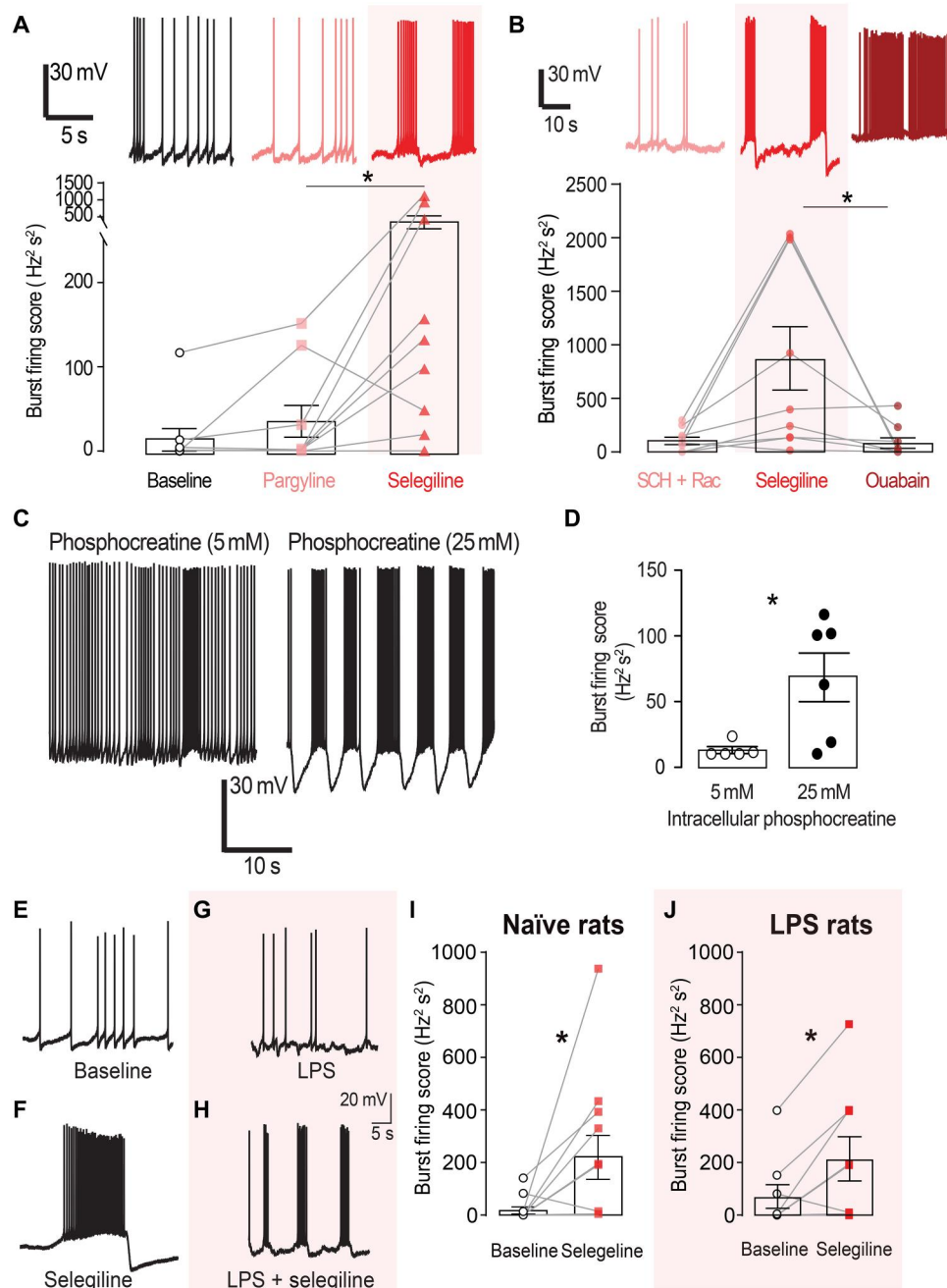
Fig. 4. The MAO-B inhibitor selegiline enhances burst-pause firing in CINs. (**A**) Selegiline (100 μM), and not pargyline (100 μM), significantly increased burst-pause firing in CINs (n = 9). (**B**) The selegiline-induced (100 μM) increase in burst-pause firing persisted in the presence of SCH23390 (SCH; 10 μM) and raclopride (Rac; 10 μM) but was abolished by ouabain (100 μM; n = 9). (**C**) Raw traces showing that a higher concentration of phosphocreatine (25 mM) in the recording pipette significantly increased burst-pause firing in CINs. (**D**) Grouped data for 5 mM (n = 5) and 25 mM (n = 6) phosphocreatine in the intracellular solution. (**E** and **F**) Selegiline increased burst-pause firing in CINs in untrained naïve rats (n = 11) and (**G** and **H**) in rats with LPS injected into the Pf (n = 9). (E) to (H) show raw traces, and (**I**) and (**J**) show grouped data. Error bars represent ±1 SEM. *P < 0.05.

selegiline during reversal training performed similarly to controls (Fig. 5F). Contrast analysis again supported these observations: There was an overall devaluation effect $F(1,30) = 28.22$, $P < 0.001$. We found that the size of the devaluation effect in the two saline groups (Sal Sal versus Sal SEL) did not differ ($Fs < 1$) and nor did it differ that these controls were compared with the LPS group that

received selegiline (LPS SEL; $F < 1$). However, the devaluation effect in these three groups combined (Sal Sal + Sal SEL + LPS SEL) differed significantly from the LPS Sal group, $F(1,30) = 4.716$, $P = 0.038$. Comparison between devalued and valued levers revealed a reliable simple effects in the Sal Sal group, $F(1,30) = 11.125$, $P = 0.002$; the Sal SEL group, $F(1,30) = 9.523$, $P = 0.004$; and the LPS

LPS + peripheral selegiline
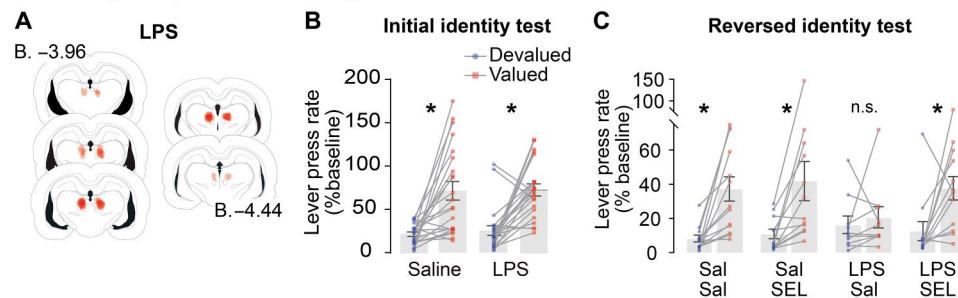
LPS + intra pDMS selegiline
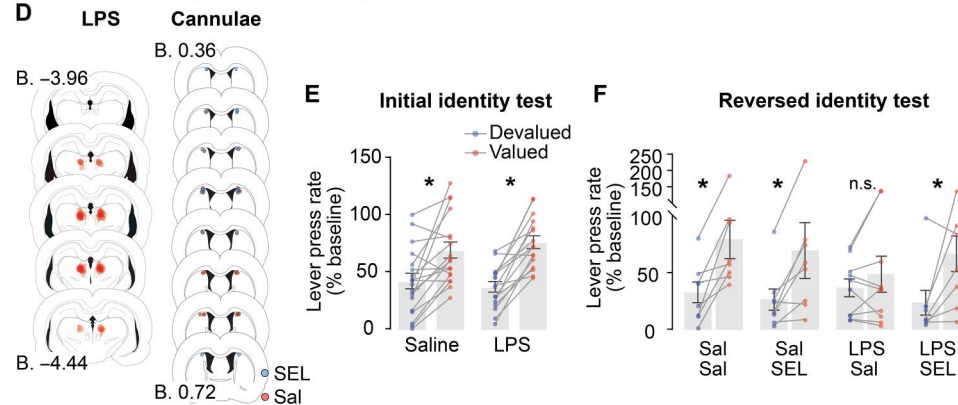
NMDA + peripheral selegiline
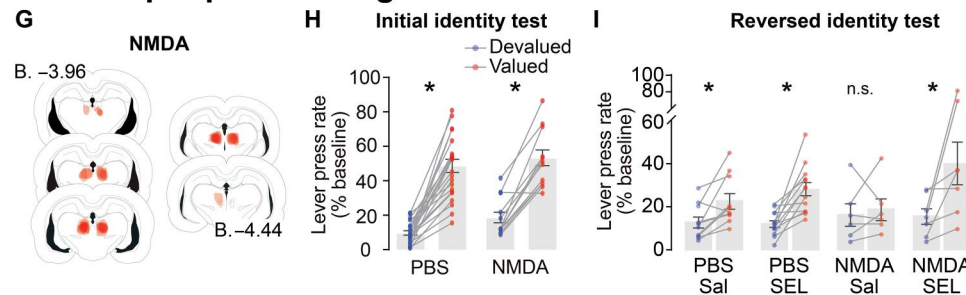
Fig. 5. AO contingency update impairment can be rescued by administration of selegiline. (**A**) Reconstruction of LPS lesion in the Pf. (**B**) Lever press rate during outcome devaluation expressed as percentage to responding during training (% baseline) following initial AO identity in rats that received bilateral injections of either saline or LPS in the Pf and (**C**) after the reversed identity training, where saline (Sal Sal and LPS Sal) or selegiline (Sal SEL and LPS SEL) was administered systemically before each reversal training session. Sal Sal, $n = 13$; Sal SEL, $n = 11$; LPS Sal, $n = 12$; LPS SEL, $n = 10$. (**D**) Maps of LPS infusions in the Pf and cannula placements in the pDMS. (**E**) Lever press rate during outcome devaluation as percentage baseline following initial AO identity training in rats that received bilateral injections of either saline or LPS in the Pf and (**F**) after the reversed identity training where saline (Sal Sal and LPS Sal) or selegiline (Sal SEL and LPS SEL) was infused in the pDMS before each reversal training session. Sal Sal, $n = 8$; Sal SEL, $n = 8$; LPS sal, $n = 10$; LPS SEL, $n = 8$. (**G**) Spread of NMDA lesion in the Pf. (**H**) Lever press rate during outcome devaluation as percentage baseline following the initial AO identity training in rats that received bilateral injections of either NMDA or PBS in the Pf and (**I**) after the reversed identity training where saline (PBS Sal and NMDA Sal) or selegiline (PBS SEL and NMDA SEL) was administered systemically before each reversal training session. PBS Sal, $n = 10$; PBS SEL, $n = 13$; NMDA Sal, $n = 6$; NMDA SEL, $n = 7$. Error bars represent ±1 SEM. *$P < 0.05$.

SEL group, $F(1,30) = 9.483$, $P = 0.004$; but not in the LPS Sal group, $F < 1$, $P > 0.05$.

Last, we sought to extend these findings and assess whether selegiline was able to reverse the behavioral impairment in encoding flexibility previously observed in another model of thalamic degeneration induced by the infusion of a cytotoxic concentration of NMDA into the Pf (*4*). Rats received bilateral injections of NMDA or phosphate-buffered saline (PBS) into the Pf (Fig. 5G). In a subset of rats that received NMDA, we first assessed the

effect of selegiline on CIN firing and found that incubation of selegiline with NMDA-lesioned brain slices induced burst firing activity (fig. S5D). Next, we trained and tested the remaining rats on the same behavioral protocol as described in the previous experiments (Fig. 5, H and I, and fig. S5E). NMDA lesions had no effect on the initial acquisition of goal-directed behavior (Fig. 5H), generating a main effect of devaluation $F(1,34) = 158.9$, but neither an effect of group $F(1,34) = 3.324$, $P > 0.05$ nor a group × devaluation interaction $F < 1$. In the final devaluation test after reversal learning,

however, we found a deficit in the NMDA-lesioned rats that received saline injections during reversal training (NMDA Sal; Fig. 5I) that was, again, ameliorated in rats that received injections of selegiline during reversal training (NMDA SEL). Contrast analysis revealed an overall devaluation effect $F_{(1,32)} = 24.813$, $P < 0.001$, and a main effect of selegiline $F_{(1,32)} = 6.962$, $P = 0.013$, but no difference in the size of the devaluation effects in the control groups (PBS Sal versus PBS SEL) or when these groups were combined and compared to the NMDA SEL group, $Fs < 1$. However, the three groups (PBS Sal + PBS SEL + NMDA SEL) compared to NMDA Sal generated a group × devaluation interaction $F_{(1,32)} = 4.406$, $P = 0.044$. Comparison between devalued and valued levers revealed a reliable simple effect for the PBS Sal group, $F_{(1,32)} = 4.307$, $P = 0.046$; the PBS SEL group $F_{(1,32)} = 14.281$, $P < 0.001$; and the NMDA SEL group, $F_{(1,32)} = 18.125$, $P < 0.001$; but no difference for the NMDA Sal group, $F_{(1,31)} < 1$.

DISCUSSION

For goal-directed actions to remain adaptive, specific AO relationships have to be learned and encoded in such a manner that they can be individually retrieved without interfering with each other. Any such interference would be highly maladaptive: It would render the consequences of actions uncertain, hinder decision-making, and block, or at least make more tenuous, action selection particularly when contingencies become uncertain in a changing context. The current experiments explored the role of the thalamostriatal pathway in AO encoding in these changing circumstances using an outcome identity reversal task designed to discriminate failures of AO learning from effects on attention or novelty/familiarity. Using this task, we found that this pathway was necessary to remap or update current AO learning but was not necessary for performance after such encoding, confirming the role of this pathway in allowing newly acquired AO associations to be encoded without interference from those already encoded. These findings suggest that neurological conditions resulting in degeneration of this pathway will have substantial effects on goal-directed action control. We evaluated this prediction using neuroinflammation and NMDA-induced cytotoxicity models of degeneration and found direct evidence that degeneration of this pathway abolished goal-directed control but only when animals were forced to update previous learning. The projection from the thalamus likely has many effects, but we found that its influence on AO encoding depends predominantly on its influence on cholinergic activity in the pDMS, particularly on the firing activity of CINs. Last, we found that the influence of this degeneration could be ameliorated by correcting its effects on CIN firing, providing a treatment for the degeneration-induced cognitive deficits resulting in the maladaptive control of goal-directed action.

More specifically, we first established that, using an hM4 DREADD expressed on pDMS projecting neurons in the Pf, activity in the Pf-pDMS pathway is necessary during the encoding of newly acquired AO associations but appeared to be less necessary during their retrieval. We then investigated the influence of neuroinflammation in the Pf, induced by the infusion of LPS, on AO encoding. We found that LPS caused considerable changes in Pf and degeneration of the thalamostriatal pathway, similar to that we found in the case of dopamine neurons when infused into the substantia nigra (46). However, it did not affect initial AO encoding and only

abolished the ability of rats to encode AO associations after AO associations changed during outcome identity reversal, as we found previously after NMDA lesions of the Pf (4, 5). At the thalamostriatal cellular level, it is clear that Pf neurons are not homogenous (47, 48). A broad classification describes most neurons in the Pf as having a "reticular or diffuse" type of dendritic morphology, with the remainder having a "bushy" morphology that resembles classic relay neurons (47, 48). Our Pf-pDMS projection neuron sampling, using electrophysiological recording and post hoc morphological staining, was able to confirm this diffuse/bushy classification (Fig. 1E and fig. S1E). Consistent with the existing literature, we found more diffuse (16 of 21; 76%) Pf cells projecting to pDMS, compared with bushy (5 of 21; 24%) Pf neurons sampled. With regard to lesion-induced damage, whereas NMDA lesions within the Pf induced complete cellular destruction, LPS lesions produced more partial effects, and we often found patches of functional neurons, something that is reminiscent of the effects observed in patients with PD. In humans, neurons in the centromedian/Pf region that project to the putamen and caudate contain both parvalbumin-positive and calbindin-positive neurons that exhibit differential susceptibility to degeneration. In PD, there is considerable loss of parvalbumin-positive neurons in the Pf region, whereas parvalbumin-negative neurons appear to be less affected (16). We examined these viable patches within the LPS lesion perimeter but found no selectivity in the type of healthy Pf neurons that remained, diffuse 16 of 20 versus bushy 4 of 20, which were similar cell type percentages to those in nonlesioned subjects (49). Although we did not assess the selectivity of LPS-induced degeneration based on parvalbumin immunoreactivity, the distribution of parvalbumin neurons in rodent Pf appears to be quite different from primates and humans, with only few neurons in rodent Pf labeled from in situ hybridization and immunohistochemistry (50–52). None of the Pf neurons recorded from the present study displayed fast-spiking capability, a hallmark of parvalbumin neurons in the central nervous system (53). Nevertheless, note that while partial neurodegeneration is a common feature in various neurological diseases, including PD, this does not appear to reflect a selective loss of a single cell type in these diseases. Pf neurons also innervate other brain structures, such as subthalamic nucleus and nucleus accumbens via noncollateralizing pathways (49). However, our disconnection evidence suggested that, unlike the Pf-DMS pathway, these projections do not play a critical role in instrumental learning after outcome identity reversal, and likely play an important role in other functions, including motivational and motor learning in conjunction with the specific topographical cortical innervation of the Pf (27, 49).

Within the rat putamen, vGlut2 expression is predominantly observed in thalamostriatal projections (54). Our research findings indicate that the infusion of LPS in the Pf resulted in the loss of neurons projecting to the pDMS, along with a reduction in synaptic puncta intensity. Unexpectedly, this loss did not correspond to any changes in vGlut2-positive terminals in the striatum, a result that is, nevertheless, consistent with similar studies conducted in monkeys subjected to MPTP treatment (55). Furthermore, vGlut2 expression has been reported to increase in the putamen of patients with PD and PD animal models (56–58), suggesting that compensatory mechanisms may be at work in PD conditions. The lack of changes in vGlut2 expression may, therefore, be attributed to various factors. First, incomplete lesioning within the local injection

sites of Pf by LPS may have resulted in less-severe neurodegeneration. Second, the abundance of other vGlut2 thalamic terminals in the DMS may have made our immunostaining and quantification of vGlut2 expression less sensitive to detect differences. Moreover, other thalamic nuclei may have increased their striatal innervation to compensate for the loss of Pf-pDMS projections. Third, vGlut2 expression has been observed to increase in dopaminergic neurons in response to cellular stress (56), again suggesting possible compensatory mechanisms in the striatum. Last, it is possible that our sampled area for quantification did not correspond to the high Pf input terminal section of DMS (59), because we did not specifically target striatal patch or matrix. vGlut2-positive terminals in striatal patch and matrix are organized differently, with a substantially larger percentage of axodendritic synapses in the matrix compartment (60). This could indicate a greater targeting of aspiny striatal interneurons (e.g., CINs) (61, 62), coinciding with most of these interneurons being found in the striatal matrix compartment in adult animals (63, 64).

At a cellular level, activity in the thalamostriatal projection has been found to induce a burst-pause firing pattern in CINs (35, 36, 65), and we were able to replicate this effect using ChR2 infused into the Pf and stimulating Pf inputs to the pDMS. Guided by this finding, we then sought to decouple the Pf input and its effects on CIN activity using an asymmetrical disconnection approach. We infused LPS unilaterally into the Pf in one hemisphere and inhibited striatal CIN activity in the contralateral striatum using the cholinergic M2/M4 autoreceptor agonist Oxo-S. Relative to controls, disconnection had a similar functional effect to bilateral LPS and blocked AO encoding after outcome identity reversal. Although the mechanics of burst firing are intrinsic to CINs (41, 42), an important role for the thalamostriatal input may be to initiate this burst-pause activity under specific conditions or after changes in state (31, 66), such as that induced by a shift in AO contingency. Consistent with this hypothesis, we found that, in an ex vivo slice preparation, CINs exhibited significantly more burst-pause firing immediately after reversed contingency training than in rats maintained under the original contingency. Concurrently, p-S6rp immunoreactivity at residues 240 to 244 in CINs was elevated in the reversed contingency group. Conversely, CINs recorded in slices taken from rats with LPS infused into the Pf showed reduced p-S6rp immunoreactivity and decreased spontaneous firing. Although these effects on p-S6rp were small and their functional significance is not fully understood, these measures together suggest that activity in the thalamostriatal pathway was sufficient to provide the necessary excitatory drive to induce striatal CINs to fire in a burst-pause pattern and so to modulate plasticity during reversed contingency learning.

The burst-pause action potential firing in CINs is known to be at least partially regulated by dopamine (36), and we evaluated its role by comparing the effects of the selective MAO-B inhibitor selegiline with that of the MAO-A/B inhibitor pargyline on CIN firing. We found that selegiline, but not pargyline, could induce burst-pause firing in CINs from ex vivo striatal slices taken from untrained naïve rats. However, unexpectedly, this effect appeared not to be dependent on dopamine activity: Selegiline was found to continue to induce burst-pause activity in the presence of dopamine D1 and D2 antagonists. Furthermore, we found that selegiline was able to normalize burst-pause firing in CINs on slices taken from rats given LPS infusions into the Pf.

Selegiline does have other pharmacological actions, although less well reported. Perhaps its most important function is as an enhancer of sodium-potassium ATPase activity, an energy-demanding enzyme, which consumes a large amount of ATP to maintain electrogenicity and excitability in mammalian cells (67). This suggests that selegiline may induce its effects by increasing intracellular ATP to stimulate sodium-potassium ATPase activity and ultimately burst firing in CINs. In support of this hypothesis, we found that ouabain, an inhibitor of sodium-potassium ATPase, abolished selegiline-induced burst firing. By contrast, elevating intracellular ATP level via incorporation of the ATP regenerative agent phosphocreatine inside the recording pipette significantly increased burst firing in CINs. Unfortunately, ouabain affects all mammalian cells, and we have so far been unable to induce a change in sodium-potassium ATPase that is limited to CINs. Burst-pause firing in CINs involves activation of many calcium channels and calcium stores (68). While blocking calcium entry and depleting stores can inhibit burst-pause firing in CINs from ex vivo brain slice experiments, these drugs can also directly affect activity of spiny projection neurons. Last, the spontaneous firing of CINs is critically dependent on normal functioning of a number of ion channels, and the cationic channel I_h has been attributed to the spontaneous depolarization phase needed by CINs for their unique spontaneous activity (69, 70). We found that selegiline had no effect on I_h in CINs.

Together, these data suggested that selegiline may be able to reverse the functional effects of LPS-induced degeneration of the thalamostriatal pathway on a goal-directed action, specifically on AO encoding after changes in the AO contingency. To assess this, we first examined the effect of peripherally administered selegiline in rats given either LPS-induced or NMDA-induced degeneration of the Pf. We found that injections of selegiline during newly acquired learning, when outcome identities were reversed, rescued the ability of rats to accurately encode these reversed contingencies as assessed in a subsequent outcome devaluation test. We found a similar effect when selegiline was administered centrally directly into the pDMS, confirming the locus of selegiline's effect.

Selegiline (also known as L-deprenyl) has been used clinically as an adjunct to treat early-stage PD in an attempt to delay the introduction of L-dopa for control of motor movement. Its effect on the cognitive effects of PD or other dementias is more equivocal with some studies reporting an improvement and others reporting ambiguous results. This is understandable given the dementia disease variants recruited in these studies, mostly with unknown neurological degeneration characteristics. While our investigations demonstrated a substantial improvement in encoding newly introduced AO contingencies, it will be important to extend these findings to other capacities. In accord with our attempt to establish the specific function of the thalamostriatal pathway and its role in controlling striatal activity, our experiments applied manipulations to healthy CINs, as validated by electrophysiological recordings from test subjects, with only one brain region inactivated at a given time. In human drug trials, there is often multifocal neuronal degeneration in the diseased brain, and this could reduce the effectiveness of drugs, such as selegiline, in overcoming deficits, producing mixed results. Therefore, it will be important to investigate the effects of selegiline in broader disease models. Nevertheless, the results of the current study, in which selegiline was able to completely reverse the effects of a deficit in a complex cognitive learning process mediating a goal-directed action, appear promising and

suggest a potential drug treatment for neuroinflammation-induced cognitive decline.

MATERIALS AND METHODS
Study design
The objective of this study was to explore the effect of inflammation in the Pf on the Pf-pDMS pathway and the encoding of newly acquired AO associations for goal-directed action. We first used a chemogenetic approach to inactivate the Pf-pDMS pathway during newly acquired AO learning. Subsequently, we used LPS-induced inflammation in the Pf to induce inactivation and a disconnection approach to confirm this inflammation-affected striatal cholinergic activity. Next, we assessed the importance of CINs in the pDMS for the encoding of newly acquired AO associations, and using ex vivo electrophysiology, we examined the effect of newly acquired AO learning on CINs burst firing. In a series of ex vivo studies, we then assessed whether selegiline affects CIN burst firing and the cellular basis for this effect before assessing whether either intraperitoneal or intrastriatal selegiline could rescue the behavioral deficits induced by bilateral LPS- and NMDA-induced degeneration of the Pf. Some animals were excluded from the analysis based on histological assessment. The final number of samples is indicated in the figure legends. In electrophysiological and immunohistochemical analyses, investigators were blind to the experimental group.

Study approval
All procedures were approved by the University of New South Wales Ethics Committee. All animal studies reported are in compliance with the ARRIVE guidelines (71, 72).

Animals
Female and male Long-Evans rats, weighing between 250 and 350 g in females and 400 and 500 g in males at the beginning of the experiment, were used as subjects. Rats that experienced behavioral training and testing were maintained at ~85% of their free-feeding body weight by restricting their food intake to between 8 and 12 g of their maintenance diet per day.

Surgeries
Rats were anesthetized with isofluorane (5% for induction and 2 to 3% for maintenance) and positioned in a stereotaxic frame (Kopf, model 942). An incision was made to expose the scalp of the rats, and an incisor bar was adjusted to align bregma and lambda on the same horizontal plane. For all rats, holes were drilled into the skull above the appropriate targeted structures using coordinates in millimeters and relative to bregma and skull. Before the start of the surgery, the animals received injections of an antibiotic [Benacillin; 0.3 to 0.4 ml, subcutaneously (sc)] and a local anesthetic (bupivicaine; 0.1 ml, sc) at the surgical site. During surgery, rats received an injection of an analgesic (carprofen; 0.03 to 0.04 ml, sc) and warm saline [5 ml, intraperitoneally (ip)].

For behavioral experiments, microinfusions were delivered using a microinjector (Harvard Apparatus, 11 Elite) using a 1- or 5-μl Hamilton syringe at an infusion rate of 0.1 μl/min. After each injection, the needle was left in situ for an additional 6 min to avoid reflux along the injection track. In the pDMS [−0.1 mm anteroposterior (AP), ±2.5 mm mediolateral (ML), −4.7 mm dorsoventral (DV)] (73), rats received injections of AAV5.CMV.HI.eGFP-Cre.WPRE.SV40 (Addgene, #105545; 0.3 μl). In the Pf (females: −4.1 mm AP, ±1.3 mm ML, −6.1 mm DV; males: −4.4 mm AP, ±1.3 mm ML, −6.55 mm DV) (73), rats received injections of LPS (Sigma-Aldrich, #L2880; 5 mg/ml in sterile saline, 1.2 μl), NMDA (Sigma-Aldrich, #M3262; 10 mg/ml in sterile PBS 0.1 M, 0.5 μl) or AAV5-hSyn-DIO-hM4D-mCherry (Addgene, #44362; 0.75 μl). Rats in control groups received rAAV5/hSyn-DIO-mCherry (Addgene, #50459; 0.75 μl), saline (1.2 μl), or sterile PBS (0.5 μl). For ex vivo electrophysiology, Pf and centrolateral thalamic nucleus (CL) were injected with AAV5-hSyn-hChR2(H134R)-eYFP (Addgene, #26973; 0.50 μl for Pf and 0.25 μl for CL). In female rats, CL coordinates were −3.6 mm AP, ±1.3 mm ML, and −5.6 mm DV.

For retrograde tracing, rats received microinjections of 3% FG in the pDMS (−0.5 mm AP, +2.5 mm ML, −4.7 mm DV) (73). In this experiment, FG and LPS were delivered via a glass micropipette attached to the end of a Nanoject (Drummond Scientific Company, Nanoject II). Six 18.4 nl of FG (List Labs, #104) or 17 × 69 nl of LPS were injected at 30-s intervals. The micropipette was left in place for a further 10 min to allow the solution to diffuse. AAV5.CMV.-HI.eGFP-Cre.WPRE.SV40 (Addgene, #105545; 0.3 μl) was infused in the pDMS and AAV2/5-hSyn-FLEX-mGFP-2A-Synaptophysin-mRuby (Addgene, #71760-AAV1; 0.7 μl) in the Pf at a rate of 0.1 μl/min using Nanoject (Drummond Scientific Company, Nanoject III).

For intracranial infusions of Oxo-S and selegiline in the pDMS, rats received a 26-G guide cannula (P1 Technologies, #C315GRL/SP) implanted above the pDMS. The tip of the guide cannula was aimed at 1 mm above the target region (i.e., −0.0 mm AP, ±2.5 mm ML, and −3.5 mm DV) (73). The guide cannulas were maintained in position with screws and dental cement, and dummy cannulas were kept in each guide at all times except during microinfusions. At the time of infusions, 33-G infusion cannulas (P1 Technologies, #C315I/SP) were lowered, and Oxo-S (Sigma-Aldrich, #O9126; 1 μM, 1 μl), selegiline (Sigma-Aldrich, #M003; 1 mM, 1 μl), or saline (1 μl) was infused using a syringe pump (Harvard Apparatus, PHD Ultra) at a rate of 0.4 μl/min with 2-min diffusion before being removed.

Behavioral procedures
Training and devaluation
Magazine training. On day 1, all rats were placed in operant chambers for approximately 20 min. In each session of each experiment, the house light was illuminated at the start of the session and turned off when the session was terminated. No levers were extended during magazine training. Twenty grain pellets and 20 20% sucrose solution outcomes were delivered to the magazine port on an independent random time 60-s schedule.

Lever training. The animals were next trained to lever press on random ratio schedules of reinforcement. Each lever was trained separately each day, and the specific lever-outcome assignments were fully counterbalanced. The session was terminated after 20 outcomes were earned or after 30 min. For the first 2 days, lever pressing was continuously reinforced. Rats were shifted to a random ratio 5 (RR5) schedule for the next 2 days (i.e., each action delivered an outcome with a probability of 0.2) and then to an RR10 schedule (or a probability of 0.1) for 3 days.

Devaluation extinction tests. After the final day of RR10 training, rats were given free access to either the pellets or the sucrose

solution for 45 min in the devaluation cage. The aim of this prefeeding procedure was to satiate the animal specifically on the prefed outcome, thereby reducing its value relative to the non-prefed outcome (29). Rats were then placed in the operant chamber for a 5-min choice extinction test. During this test, both levers were extended and lever presses were recorded, but no outcomes were delivered. The next day, a second devaluation test was administered with the opposite outcome. Rats were then placed back into the operant chambers for a second 5-min choice extinction test.

Contingency reversal training. Subsequent to the extinction test, rats were trained to lever press on an RR10 schedule, with the previously trained contingencies reversed. That is, the lever that previously earned grain pellets now earned sucrose solution, and the lever that previously earned sucrose solution now earned pellets. Contingency reversal training continued for 4 days.

Immunofluorescence

Rats were anesthetized with sodium pentobarbital (150 mg/kg, ip; Virbac Pty. Ltd., Australia) and transcardially perfused with 400 ml of 4% paraformaldehyde (PFA) in sodium phosphate buffer [0.1 M PB (pH 7.4)]. Brains were postfixed overnight in 4% PFA PB and stored at 4°C. Coronal sections (35 μm) were cut with a vibratome (Leica Microsystems, VT1000) and stored at −20°C in a solution containing 30% ethylene glycol, 30% glycerol, and PB, until they were processed for immunofluorescence.

Free-floating sections were rinsed in tris-buffered saline with sodium fluoride [TBS-NaF; 0.25 M tris, 0.5 M NaCl, and 0.1 mM NaF (pH 7.5)], incubated for 5 min in TBS-NaF containing 3% H_2O_2 and 10% methanol, and then rinsed for 10 min three times in TBS-NaF. After 20 min of incubation in 0.2% Triton X-100 in TBS-NaF, sections were rinsed three times in TBS-NaF again. ChAT and the double p-S6rp (p-Ser$^{240-244}$-S6rp) were simultaneously detected through incubation with combined polyclonal goat anti-ChAT (1:500; #AB144P, Millipore) and polyclonal rabbit anti–p-Ser$^{240-244}$-S6rp (1:500; #2215, Cell Signaling Technology) primary antibodies diluted in TBS-NaF (4°C, overnight). NeuN and Iba1 were simultaneously detected through incubation with combined polyclonal mouse anti-NeuN (1:1000; #MAB377, Merck) and polyclonal goat anti-Iba1 (1:1000; #AB5076, Abcam) primary antibodies diluted in TBS (4°C, overnight). Sections were then rinsed for 10 min in TBS three times and incubated for 60 min with donkey anti-goat Alexa Fluor 594 (#A11058, Invitrogen) and donkey anti-mouse Alexa Fluor 488 (#A21202, Invitrogen) secondary antibodies diluted 1:1000 in TBS. Sections were rinsed four times for 10 min in TBS before being mounted on slides and coverslipped with Vectashield fluorescence medium (H-1000-10, Vector Laboratories).

Another set of Pf sections with LPS injection were double stained with FG, NeuN, and Iba1 through incubation with combined polyclonal mouse anti-NeuN (1:1000; #MAB377, Merck) and polyclonal goat anti-Iba1 (1:1000; #AB5076, Abcam) primary antibodies diluted in TBS (4°C, overnight). Sections were then rinsed for 10 min in TBS three times and incubated for 60 min with donkey anti-goat Alexa Fluor 647 (#A32849, Invitrogen) and donkey anti-mouse Alexa Fluor 546 (#A10036, Invitrogen) secondary antibodies diluted 1:500 in TBS. Sections were rinsed four times for 10 min in TBS before being mounted on slides and coverslipped with Vectashield fluorescence medium (H-1000-10, Vector Laboratories). A set of pDMS sections were stained with a rabbit anti-vGlut2

(1:500; #93624S, Cell Signaling) primary antibody and donkey anti-rabbit Alexa Fluor 647 (#A31573, Invitrogen).

Fluorescence analysis and cell count images were obtained using sequential laser scanning confocal microscopy (Fluoview FV1000, BX61WI microscope, Olympus). All ChAT-immunoreactive neurons in dorsomedial and dorsolateral striatal regions were detected in the microscope using a ×60 objective (UPFL 60× oil) and centered on the acquisition area. Focal plane with optimal ChAT immunoreactivity was determined in channel 2 (Ch02; HeNe green laser). Sequential high-resolution images (optical magnification: ×60; digital zoom: ×4; resolution: 1024 px by 1024 px) were obtained for p-Ser$^{240-244}$-S6rp signal (Ch01) and corresponding ChAT signal (Ch02) with a Kaplan filter (five averaging scans). Laser intensity, photomultiplier tube voltage, and offset were maintained constant in all acquisitions of the same experiment. Raw 16-bit images were then analyzed using ImageJ software (MacBiophotonics upgrade v. 1.43u; W. Rasband, National Institutes of Health, USA). In superimposed channels, somatic neuronal area (excluding the nucleus) was determined as a region of interest (ROI) in Ch02 (ChAT signal), and mean fluorescence intensity (mean gray value; gray values ranging from 0 to 255) was measured in corresponding Ch01 (p-Ser$^{240-244}$-S6rp signal). A pseudo-color palette highlighting intensity of fluorescence (16-color lookup table; display range: 0 to 255) was applied to representative neurons.

NeuN-positive neurons in the Pf region were quantified as follows: High-resolution scanning confocal images of Pf were obtained from unilateral LPS-injected rats or control rats, imaging the same coronal level (optical magnification: ×10; resolution: 2048 px by 2048 px). NeuN-positive cell counts were performed using ImageJ software (cell counter plug-in). Before all quantifications, all image files in each experiment were randomly renumbered using an MS Excel plug-in (Bio-excel2007 by R. Bouju, France). An ROI of the Pf was drawn to exclude the needle track in LPS-injected sides, and the image was converted to 8-bit. A thresholding was calculated; then, after applying a Gaussian blur filter (sigma radius of 1), the image was made binary and the watershed plug-in was applied. The cell counter plug-in calculated the neurons that were in the size range of 50 to 400 μm^2 and circularity of 0.20 to 1.00. Iba1 staining was used to show the effect of LPS and to assess correct placements of injections.

Brain slice preparation

Rats were euthanized under deep anesthesia (isoflurane 4% in air), and their brains were rapidly removed and cut on a vibratome in ice-cold oxygenated sucrose buffer containing the following: 241 mM sucrose, 28 mM NaHCO$_3$, 11 mM glucose, 1.4 mM NaH$_2$PO$_4$, 3.3 mM KCl, 0.2 mM CaCl$_2$, and 7 mM MgCl$_2$. Coronal brain slices (300-μm thick) containing the pDMS or Pf were sampled and maintained at 33°C in a submerged chamber containing physiological saline with composition as follows: 130 mM NaCl, 2.6 mM KCl, 1.4 mM NaH$_2$PO$_4$, 1.2 mM MgCl$_2$, 2.5 mM CaCl$_2$, 12 mM glucose, and 27 mM NaHCO$_3$, and equilibrated with 95% O$_2$ and 5% CO$_2$.

Electrophysiology

After equilibrating for 1 hour, slices were transferred to a recording chamber, visualized under an upright microscope (Olympus, BX50WI) using differential interference contrast (DIC) Dodt tube optics, and superfused continuously (1.5 ml min^{-1}) with oxygenated physiological saline at 33°C. Cell-attached and whole-cell patch-clamp recordings were made using electrodes (2 to 5 megohm)

containing internal solution consisting of the following: 115 mM K gluconate, 20 mM NaCl, 1 mM MgCl$_2$, 10 mM Hepes, 11 mM EGTA, 5 mM phosphocreatine di(tris) salt (#P1937, Sigma-Aldrich), 5 mM Mg-ATP, and 0.33 mM Na–guanosine triphosphate (pH 7.3), with osmolarity of 285 to 290 mOsm liter^{-1}. Biocytin (0.1%; #B4261, Sigma-Aldrich) was added to the internal solution for marking the sampled neurons during whole-cell recording. Data acquisition was performed with a Multiclamp 700B amplifier (Molecular Devices), connected to a Macintosh computer and interface ITC-18 (InstruTech). Action potential deflections in a cell-attached configuration and voltage/current recordings under a whole-cell configuration were sampled at 5 kHz (low-pass filter of 2 kHz; AxoGraph X, Molecular Devices). Data from cell-attached and whole-cell recordings were only included in analyses if (i) the neurons appeared healthy under DIC on the monitor screen, (ii) CINs were spontaneously active during the cell-attached recording, (iii) action potential amplitudes were at least 60 mV above threshold after establishing the whole-cell recording mode, and (iv) neurons demonstrated the physiological characteristics of CINs such as the presence of hyperpolarization-activated cation current I_h but no plateau low-threshold spiking (70), to ensure that only highly viable neurons were included. Liquid junction potentials of −10 mV were not corrected. All current-clamp data were recorded at resting membrane potential.

Action potential analysis
To calculate an aggregate as "burst firing score" for each neuron, in AxoGraph X, the variance of spike (or action potential) instantaneous frequency is multiplied by variance of interspike interval. Baseline was taken as just before drug application (analysis of 200 spikes), while drug effect was typically taken around the 5- to 10-min mark during application (analysis of 200 spikes). For a CIN that undergoes intense burst firing, there will be a large variance in spike frequency and also a large variance in interspike interval. In ouabain, drug effect was taken after 1.5 min because action potentials completely disappeared after 5 min of application.

Post hoc histology
Immediately after physiological recording, brain slices containing biocytin-filled neurons were fixed overnight in 4% PFA/0.16 M PB solution and then placed in 0.5% Triton X-100/PB for 3 days to permeabilize cells. Slices were then placed in 10% horse serum/PB for 1 hour before being incubated in primary goat anti-ChAT (1:500; #AB144P, Merck) for 2 days at 4°C to aid identification of CINs. The slices were rinsed in PB and then, in a one-step incubation, containing both Alexa Fluor 647–conjugated donkey anti-goat secondary antibody (1:500; #A21447, Invitrogen) and Alexa Fluor 488–conjugated streptavidin (1:1000; #S11223, Invitrogen) for 2 hours. For slices containing Pf neuron with mCherry labeling, after cell permeation with Triton X-100, they were incubated only in Alexa Fluor 488–conjugated streptavidin (1:1000; #S11223, Invitrogen) for 2 hours. For slices containing Pf neuron in LPS rats, they were incubated in goat anti-Iba1 (1:1000) overnight at room temperature, followed by donkey anti-goat Alexa Fluor 488 (1:500; #A11055, Invitrogen) and ExtrAvidin-Cy3 (1:500; #E4142, Sigma-Aldrich) at room temperature for 4 hours. Stained slices were rinsed in PB three times for 10 min each, mounted/dried on a glass slide, and coverslipped with Fluoromount-G mounting medium (#0100-01, Southern Biotech). Neurons were imaged under a confocal microscope (Fluoview FV1000 and BX61WI, Olympus).

Drugs
All the following drugs, except CNO, were purchased from Sigma-Aldrich, St. Louis, MO. Working drug concentrations are as follow: LPS (O55:B5, L2880, Sigma-Aldrich; 5 mg/ml dissolved in PBS, 1 μl), oxotremorine sesquifumarate (Oxo-S, #O9126, Sigma-Aldrich; 1 μM dissolved in PBS), selegiline [R(−)-deprenyl HCl, #M003, Sigma-Aldrich; 1 mg/kg, ip, and 1 mM, 1 μl infused in the pDMS], CNO (RTI International, custom synthesis batch no. 13626-76; 7 mg/kg, ip). Drugs for electrophysiology are as follows: selegiline (100 μM), R(+)-SCH23390 HCl (D054, 10 μM), S(−)-raclopride (+)-tartrate (#R121, Sigma-Aldrich; 10 μM), ouabain octahydrate (#O3125, Sigma-Aldrich; 100 μM), pargyline HCl (#P8013, Sigma-Aldrich; 100 μM), and CNO (#13626-76, RTI International; 10 μM).

Statistical analysis
Experiments with two groups were analyzed using two-tailed Student's t tests, unpaired for between subjects and paired for within subject comparisons. Experiments with more than two groups that passed normality test were subjected to one-way analysis of variance (ANOVA), two-way ANOVA, or repeated-measure two-way ANOVA, followed by Sidak's tests for multiple comparisons when an interaction was found significant. Results that did not pass the normality test were analyzed using nonparametric Friedman analysis, followed by Dunn's multiple comparisons when an effect was found significant. Behavioral data for both initial contingency and reversed contingency tests were analyzed using a contrast analysis approach using PSY software (University of New South Wales) as it allows for a more fine-grained data analysis of complex experimental designs. When an interaction was found, simple effect analysis was evaluated using PSY software. A value of $P < 0.05$ was considered statistically significant. Graphs were originated using GraphPad Prism 8. All other data were analyzed using Prism, version 8.0 (GraphPad software).

Supplementary Materials
This PDF file includes:
Figs. S1 to S5

View/request a protocol for this paper from *Bio-protocol*.

REFERENCES AND NOTES
1. J. Peak, B. Chieng, G. Hart, B. W. Balleine, Striatal direct and indirect pathway neurons differentially control the encoding and updating of goal-directed learning. *eLife* **9**, 1–28 (2020).
2. G. Hart, L. A. Bradfield, S. Y. Fok, B. Chieng, B. W. Balleine, The bilateral prefronto-striatal pathway is necessary for learning new goal-directed actions. *Curr. Biol.* **28**, 2218–2229.e7 (2018).
3. Y. Hori, Y. Nagai, K. Mimura, T. Suhara, M. Higuchi, S. Bouret, T. Minamimoto, D1-and D2-like receptors differentially mediate the effects of dopaminergic transmission on cost benefit evaluation and motivation in monkeys. *PLOS Biol.* **19**, e3001055 (2021).
4. L. A. Bradfield, J. Bertran-Gonzalez, B. Chieng, B. W. Balleine, The thalamostriatal pathway and cholinergic control of goal-directed action: Interlacing new with existing learning in the striatum. *Neuron* **79**, 153–166 (2013).
5. M. Matamales, Z. Skrbis, R. J. Hatch, B. W. Balleine, J. Götz, J. Bertran-Gonzalez, Aging-related dysfunction of striatal cholinergic interneurons produces conflict in action selection. *Neuron* **90**, 362–373 (2016).
6. S. R. Lapper, J. P. Bolam, Input from the frontal cortex and the parafascicular nucleus to cholinergic interneurons in the dorsal striatum of the rat. *Neuroscience* **51**, 533–545 (1992).

7. S. Consolo, G. Baldi, S. Giorgi, L. Nannini, The cerebral cortex and parafascicular thalamic nucleus facilitate in vivo acetylcholine release in the rat striatum through distinct glutamate receptor subtypes. *Eur. J. Neurosci.* **8**, 2702–2710 (1996).

8. S. Consolo, P. Baronio, G. Guidi, G. Di Chiara, Role of the parafascicular thalamic nucleus and N-methyl-d-aspartate transmission in the D1-dependent control of in vivo acetylcholine release in rat striatum. *Neuroscience* **71**, 157–165 (1996).

9. J. P. Bolam, B. H. Wainer, A. D. Smith, Characterization of cholinergic neurons in the rat neostriatum. A combination of choline acetyltransferase immunocytochemistry, Golgi-impregnation and electron microscopy. *Neuroscience* **12**, 711–718 (1984).

10. C. Contant, D. Umbriaco, S. Garcia, K. C. Watkins, L. Descarries, Ultrastructural characterization of the acetylcholine innervation in adult rat neostriatum. *Neuroscience* **71**, 937–947 (1996).

11. J. B. Ding, J. N. Guzman, J. D. Peterson, J. A. Goldberg, D. J. Surmeier, Thalamic gating of corticostriatal signaling by cholinergic interneurons. *Bone* **23**, 1–7 (2014).

12. B. W. Balleine, Animal models of action control and cognitive dysfunction in Parkinson's disease, in *Progress in Brain Research* (Elsevier B.V., 2022), vol. 269, pp. 227–255.

13. G. M. Halliday, Thalamic changes in Parkinson's disease. *Parkinsonism Relat. Disord.* **15**, S152–S155 (2009).

14. J. M. Henderson, S. B. Schleimer, H. Allbutt, V. Dabholkar, D. Abela, J. Jovic, M. Quinlivan, Behavioural effects of parafascicular thalamic lesions in an animal model of parkinsonism. *Behav. Brain Res.* **162**, 222–232 (2005).

15. D. Brooks, G. M. Halliday, Intralaminar nuclei of the thalamus in Lewy body diseases. *Brain Res. Bull.* **78**, 97–104 (2009).

16. J. M. Henderson, K. Carpenter, H. Cartwright, G. M. Halliday, Degeneration of the centré median-parafascicular complex in Parkinson's disease. *Ann. Neurol.* **47**, 345–352 (2000).

17. R. M. Villalba, T. Wichmann, Y. Smith, Neuronal loss in the caudal intralaminar thalamic nuclei in a primate model of Parkinson's disease. *Brain Struct. Funct.* **219**, 381–394 (2014).

18. M. A. Hely, W. G. J. Reid, M. A. Adena, G. M. Halliday, J. G. L. Morris, The Sydney multicenter study of Parkinson's disease: The inevitability of dementia at 20 years. *Mov. Disord.* **23**, 837–844 (2008).

19. A. H. V. Schapira, K. R. Chaudhuri, P. Jenner, Non-motor features of Parkinson disease. *Nat. Rev. Neurosci.* **18**, 509–509 (2017).

20. D. Aarsland, K. Andersen, J. P. Larsen, A. Lolk, P. Kragh-Sørensen, Prevalence and characteristics of dementia in Parkinson disease. *Arch. Neurol.* **60**, 387–392 (2003).

21. A. Surendranathan, J. B. Rowe, J. T. O'Brien, Neuroinflammation in Lewy body dementia. *Parkinsonism Relat. Disord.* **21**, 1398–1406 (2015).

22. G. Gelders, V. Baekelandt, A. van der Perren, Linking neuroinflammation and neurodegeneration in parkinson's disease. *J. Immunol. Res.* **2018**, 1–12 (2018).

23. T. Togo, E. Iseki, W. Marui, H. Akiyama, K. Uéda, K. Kosaka, Glial involvement in the degeneration process of Lewy body-bearing neurons and the degradation process of Lewy bodies in brains of dementia with Lewy bodies. *J. Neurol. Sci.* **184**, 71–75 (2001).

24. S. Iannaccone, C. Cerami, M. Alessio, V. Garibotto, A. Panzacchi, S. Olivieri, G. Gelsomino, R. M. Moresco, D. Perani, In vivo microglia activation in very early dementia with Lewy bodies, comparison with Parkinson's disease. *Parkinsonism Relat. Disord.* **19**, 47–52 (2013).

25. M. Deschênes, J. Bourassa, V. Doan, A. Parent, A single-cell study of the axonal projections arising from the posterior intralaminar thalamic nuclei in the rat. *Eur. J. Neurosci.* **8**, 329–343 (1996).

26. H. J. Groenewegen, H. W. Berendse, The specificity of the "nonspecific" midline and intralaminar thalamic nuclei. *Trends Neurosci.* **17**, 52–57 (1994).

27. G. Mandelbaum, J. Taranda, T. M. Haynes, D. R. Hochbaum, K. W. Huang, M. Hyun, K. Umadevi Venkataraju, C. Straub, W. Wang, K. Robertson, P. Osten, B. L. Sabatini, Distinct cortical-thalamic-striatal circuits through the parafascicular nucleus. *Neuron* **102**, 636–652.e7 (2019).

28. B. N. Armbruster, X. Li, M. H. Pausch, S. Herlitze, B. L. Roth, Evolving the lock to fit the key to create a family of G protein-coupled receptors potently activated by an inert ligand. *Proc. Natl. Acad. Sci. U.S.A.* **104**, 5163–5168 (2007).

29. B. W. Balleine, A. Dickinson, Goal-directed instrumental action: Contingency and incentive learning and their cortical substrates. *Neuropharmacology* **37**, 407–419 (1998).

30. J. Bertran-Gonzalez, B. C. Chieng, V. Laurent, E. Valjent, B. W. Balleine, Striatal cholinergic interneurons display activity-related phosphorylation of ribosomal protein S6. *PLOS ONE* **7**, e53195 (2012).

31. L. A. Bradfield, B. W. Balleine, Thalamic control of dorsomedial striatum regulates internal state to guide goal-directed action selection. *J. Neurosci.* **37**, 3721–3733 (2017).

32. P. Calabresi, D. Centonze, A. Pisani, G. Sancesario, R. A. North, G. Bernardi, Muscarinic IPSPs in rat striatal cholinergic interneurones. *J. Physiol.* **510**, 421–427 (1998).

33. V. Bernard, O. Laribi, A. I. Levey, B. Bloch, Subcellular redistribution of m2 muscarinic acetylcholine receptors in striatal interneurons in vivo after acute cholinergic stimulation. *J. Neurosci.* **18**, 10207–10218 (1998).

34. M. E. Ragozzino, E. G. Mohler, M. Prior, C. A. Palencia, S. Rozman, Acetylcholine activity in selective striatal regions supports behavioral flexibility. *Neurobiol. Learn. Mem.* **91**, 13–22 (2009).

35. Y. Smith, D. J. Surmeier, P. Redgrave, M. Kimura, Thalamic contributions to basal ganglia-related behavioral switching and reinforcement. *J. Neurosci.* **31**, 16102–16106 (2011).

36. J. B. Ding, J. N. Guzman, J. D. Peterson, J. A. Goldberg, D. J. Surmeier, Thalamic gating of corticostriatal signaling by cholinergic interneurons. *Neuron* **67**, 294–307 (2010).

37. S. Threlfell, T. Lalic, N. J. Platt, K. A. Jennings, K. Deisseroth, S. J. Cragg, Striatal dopamine release is triggered by synchronized activity in cholinergic interneurons. *Neuron* **75**, 58–64 (2012).

38. P. Deng, Y. Zhang, Z. C. Xu, Involvement of I_h in dopamine modulation of tonic firing in striatal cholinergic interneurons. *J. Neurosci.* **27**, 3148–3156 (2007).

39. P. Calabresi, B. Picconi, L. Parnetti, M. Di Filippo, A convergent model for cognitive dysfunctions in Parkinson's disease: The critical dopamine–acetylcholine synaptic balance. *Lancet Neurol.* **5**, 974–983 (2006).

40. T. Aosaki, K. Kiuchi, Y. Kawaguchi, Dopamine D_1-like receptor activation excites rat striatal large aspiny neurons in vitro. *J. Neurosci.* **18**, 5180–5190 (1998).

41. J. A. Goldberg, J. N. J. Reynolds, Spontaneous firing and evoked pauses in the tonically active cholinergic interneurons of the striatum. *Neuroscience* **198**, 27–43 (2011).

42. B. D. Bennett, C. J. Wilson, Spontaneous activity of neostriatal cholinergic interneurons in vitro. *J. Neurosci.* **19**, 5586–5596 (1999).

43. K. Lee, A. K. Dixon, T. C. Freeman, P. J. Richardson, Identification of an ATP-sensitive potassium channel current in rat striatal cholinergic interneurones. *J. Physiol.* **510**, 441–453 (1998).

44. M. Beierlein, J. R. Gibson, B. W. Connors, Two dynamically distinct inhibitory networks in layer 4 of the neocortex. *J. Neurophysiol.* **90**, 2987–3000 (2003).

45. Y. Kang, T. Notomi, M. Saito, W. Zhang, R. Shigemoto, Bidirectional interactions between H-channels and Na^+-K^+ pumps in mesencephalic trigeminal neurons. *J. Neurosci.* **24**, 3694–3702 (2004).

46. S. Becchi, A. Buson, B. W. Balleine, Inhibition of vascular adhesion protein 1 protects dopamine neurons from the effects of acute inflammation and restores habit learning in the striatum. *J. Neuroinflammation* **18**, 233 (2021).

47. Y. Smith, D. Raju, B. Nanda, J. F. Pare, A. Galvan, T. Wichmann, The thalamostriatal systems: Anatomical and functional organization in normal and parkinsonian states. *Brain Res. Bull.* **78**, 60–68 (2009).

48. J. A. Beatty, E. L. Sylwestrak, C. L. Cox, Two distinct populations of projection neurons in the rat lateral parafascicular thalamic nucleus and their cholinergic responsiveness. *Neuroscience* **162**, 155–173 (2009).

49. Y. Zhang, D. S. Roy, Y. Zhu, Y. Chen, T. Aida, Y. Hou, C. Shen, N. E. Lea, M. E. Schroeder, K. M. Skaggs, H. A. Sullivan, K. B. Fischer, E. M. Callaway, I. R. Wickersham, J. Dai, X. M. Li, Z. Lu, G. Feng, Targeting thalamic circuits rescues motor and mood deficits in PD mice. *Nature* **607**, 321–329 (2022).

50. Allen Institute for Brain Science, Allen Brain Atlas [accessed 26 April 2023]; www.brain-map.org/.

51. R. Arai, D. M. Jacobowitz, S. Deura, Distribution of calretinin, calbindin-D28k, and parvalbumin in the rat thalamus. *Brain Res. Bull.* **33**, 595–614 (1994).

52. M. R. Celio, Calbindin D-28k and parvalbumin in the rat nervous system. *Neuroscience* **35**, 375–475 (1990).

53. J. M. Tepper, F. Tecuapetla, T. Koós, O. Ibáñez-Sandoval, Heterogeneity and diversity of striatal GABAergic interneurons. *Front Neuroanat.* **4**, 150 (2010).

54. T. Kaneko, F. Fujiyama, Complementary distribution of vesicular glutamate transporters in the central nervous system. *Neurosci. Res.* **42**, 243–250 (2002).

55. R. M. Villalba, J. F. Pare, S. Lee, S. Lee, Y. Smith, Thalamic degeneration in MPTP-treated Parkinsonian monkeys: Impact upon glutamatergic innervation of striatal cholinergic interneurons. *Brain Struct. Funct.* **224**, 3321–3338 (2019).

56. W. M. Kouwenhoven, G. Fortin, A.-M. Penttinen, C. Florence, B. Delignat-Lavaud, M.-J. Bourque, T. Trimbuch, M. P. Luppi, A. Salvail-Lacoste, P. Legault, J.-F. Poulin, C. Rosenmund, R. Awatramani, L.-É. Trudeau, VGluT2 expression in dopamine neurons contributes to postlesional striatal reinnervation. *J. Neurosci.* **40**, 8262–8275 (2020).

57. T. Steinkellner, V. Zell, Z. J. Farino, M. S. Sonders, M. Villeneuve, R. J. Freyberg, S. Przedborski, W. Lu, Z. Freyberg, T. S. Hnasko, Role for VGLUT2 in selective vulnerability of midbrain dopamine neurons. *J. Clin. Investig.* **128**, 774–788 (2018).

58. H. Shen, R. A. M. Marino, R. A. McDevitt, G. H. Bi, K. Chen, G. Madeo, P. T. Lee, Y. Liang, L. M. De Biase, T. P. Su, Z. X. Xi, A. Bonci, Genetic deletion of vesicular glutamate transporter in dopamine neurons increases vulnerability to MPTP-induced neurotoxicity in mice. *Proc. Natl. Acad. Sci. U.S.A.* **115**, E11532–E11541 (2018).

59. K. D. Alloway, J. B. Smith, G. D. R. Watson, Thalamostriatal projections from the medial posterior and parafascicular nuclei have distinct topographic and physiologic properties. *J. Neurophysiol.* **111**, 36–50 (2014).

60. D. V. Raju, D. J. Shah, T. M. Wright, R. A. Hall, Y. Smith, Differential synaptology of vGluT2-containing thalamostriatal afferents between the patch and matrix compartments in rats. *J Comp Neurol* **499**, 231–243 (2006).

61. Y. Smith, D. V. Raju, J. F. Pare, M. Sidibe, The thalamostriatal system: A highly specific network of the basal ganglia circuitry. *Trends Neurosci.* **27**, 520–527 (2004).

62. T. Unzai, E. Kuramoto, T. Kaneko, F. Fujiyama, Qquantitative analyses of the projection of individual neurons from the midline thalamic nuclei to the striosome and matrix compartments of the rat striatum. *Cereb. Cortex* **27**, 1164–1181 (2017).

63. A. M. Graybiel, R. W. Baughman, F. Eckenstein, Cholinergic neuropil of the striatum observes striosomal boundaries. *Nature* **323**, 625–627

64. E. H. S. Van Vulpen, D. Van Der Kooy, Differential maturation of cholinergic interneurons in the striatal patch versus matrix compartments. *J Comp Neurol* **365**, 683–691 (1996).

65. N. Matsumoto, T. Minamimoto, A. M. Graybiel, M. Kimura, Neurons in the thalamic CM-Pf complex supply striatal neurons with information about behaviorally significant sensory events. *J. Neurophysiol.* **85**, 960–976 (2001).

66. P. Apicella, Leading tonically active neurons of the striatum from reward detection to context recognition. *Trends Neurosci.* **30**, 299–306 (2007).

67. C. Antoniades, H. Carageorgiou, S. Tsakiris, Effects of (−)deprenyl (selegiline) on acetylcholinesterase and Na(+),K(+)-ATPase activities in adult rat whole brain. *Pharmacol. Res.* **46**, 165–169 (2002).

68. J. A. Goldberg, C. J. Wilson, Control of spontaneous firing patterns by the selective coupling of calcium currents to calcium-activated potassium currents in striatal cholinergic interneurons. *J. Neurosci.* **25**, 10230–10238 (2005).

69. B. D. Bennett, J. C. Callaway, C. J. Wilson, Intrinsic membrane properties underlying spontaneous tonic firing in neostriatal cholinergic interneurons. *J. Neurosci.* **20**, 8493–8503 (2000).

70. Y. Kawaguchi, Physiological, morphological, and histochemical characterization of three classes of interneurons in rat neostriatum. *J. Neurosci.* **13**, 4908–4923 (1993).

71. C. Kilkenny, W. Browne, I. C. Cuthill, M. Emerson, D. G. Altman, Animal research: Reporting in vivo experiments: The ARRIVE guidelines. *Br. J. Pharmacol.* **160**, 1577–1579 (2010).

72. J. C. McGrath, E. Lilley, Implementing guidelines on reporting research using animals (ARRIVE etc.): New requirements for publication in BJP. *Br. J. Pharmacol.* **172**, 3189–3193 (2015).

73. G. Paxinos, C. Watson, *The Rat Brain in Stereotaxic Coordinates* (Academic Press, ed. 6, 2006).